Macrophyte-hydrodynamic interactions mediate stratification and dissolved oxygen dynamics in ponds

Ellen A. Albright[1,2], Robert Ladwig[2], and Grace M. Wilkinson[1,2]

[1] Iowa State University, Ames, Iowa, USA

[2] Center for Limnology, University of Wisconsin-Madison, Madison, Wisconsin, USA

ORCID numbers and contact information

Albright: 0000-0002-6226-9158 ealbright2@wisc.edu

Ladwig: 0000-0001-8443-1999 rladwig2@wisc.edu

Wilkinson: 0000-0003-4051-2249 gwilkinson@wisc.edu

Corresponding author: Ellen A. Albright (ealbright2@wisc.edu); 223 Hasler Laboratory of Limnology, 680 N. Park Street, Madison, WI 53706 USA

This manuscript has been submitted for publication in Limnology and Oceanography. Please note that this manuscript has not yet undergone peer-review nor been formally accepted for publication. Subsequent versions of this manuscript may have slightly different content. If accepted, the final version of the manuscript will be available via the peer-reviewed publication DOI link at the top of this webpage. Please feel free to contact the corresponding author.

Keywords: dissolved oxygen, heat flux, hydrodynamics, macrophytes, phenology, ponds, water temperature

ABSTRACT

Small waterbodies are sensitive to stressors such as eutrophication and heatwaves; however, interactions between macrophytes and hydrodynamics may mediate the effects of compounding stressors. Leveraging an ecosystem experiment and hydrodynamic model, we evaluated how macrophyte biomass, thermal structure, and dissolved oxygen (DO) responded to the interaction of episodic nutrient loading and periods of high temperatures in two temperate ponds. In one pond we experimentally added pulses of nutrients, simulating storm-driven loading (the other pond served as an unmanipulated reference). Following the first nutrient pulse both ponds experienced a 5-day period of high surface water temperatures. Macrophytes in the nutrient addition pond began to senescence mid-summer due to phytoplankton shading from the nutrient addition and heat stress while macrophytes in the reference pond followed expected seasonal patterns, senescing in early autumn. Field observations and model results indicate that macrophytes structured the thermal environment through vertical attenuation of turbulent kinetic energy and light. Macrophytes reduced the vertical extent of water column warming during the heat event by 0.25-0.5 m and maintained cooler bottom temperatures (up to 2.5 °C cooler) throughout the summer, suggesting that macrophytes may buffer small waterbodies from heatwaves. Seasonal patterns in DO saturation also followed trends in macrophyte biomass; however, during the heat event, DO saturation fell sharply (-22.4 to 50.4 %) in both ponds and remained depressed through the remainder of the summer. This experiment and modeling exercise demonstrated that macrophyte influence on turbulent flows and light are pivotal in mediating how small waterbodies respond to compounding stressors.

INTRODUCTION

Small lakes and ponds are the most abundant lentic ecosystems worldwide and sites of critical importance for freshwater biodiversity and biogeochemical cycles (Scheffer et al. 2006; Cole et al. 2007; Messager et al. 2016). Small waterbodies are active components of regional- and global-scale carbon cycling, both as sites of burial and storage (Wilkinson et al. 2018; Taylor et al. 2019) and as sources of atmospheric carbon dioxide and methane (Holgerson and Raymond 2016; Peacock et al. 2021). Small lakes and ponds enhance local and regional biodiversity, due in part to abundant macrophytes (Van Geest et al. 2003). Robust macrophyte communities support greater diversity of other taxa by providing food resources and habitat structure (Williams et al. 2004; Scheffer et al. 2006). In addition to these biotic interactions, macrophytes play a pivotal role in the ecosystem structure and function of small waterbodies. Interactions between hydrodynamics and the physical structure of macrophyte beds influence turbulent mixing, water column thermal structure, and sediment stability as well as whole-lake productivity and nutrient cycling (Carpenter and Lodge 1986; Scheffer et al. 1993; Licci et al. 2019). Despite the prevalence and importance of small, vegetated lakes and ponds, these ecosystems remain understudied (Downing 2010; Biggs et al. 2017), particularly with regards to the role of macrophyte-hydrodynamic interactions in mediating ecosystem response to stressors.

The characteristic morphometry of small waterbodies makes these ecosystems more susceptible to stressors. For example, limited water volume and shallow mean depth reduce both dilution potential and thermal inertia making small waterbodies sensitive to nutrient loading and intense heatwaves (Biggs et al. 2017; Woolway et al. 2021a; Polazzo et al. 2022). As a result, eutrophication and aquatic heatwaves may act as compounding stressors for small lakes and ponds. Aquatic heatwaves are periods of sustained high surface water temperatures relative to

local and seasonal baseline conditions (Hobday et al. 2016; Tassone et al. 2021; Woolway et al. 2021a). The frequency, duration, and intensity of aquatic heatwaves have increased over the past century as a result of anthropogenic climate change, a trend which is anticipated to continue, even under low green-house-gas-emissions scenarios (Oliver et al. 2018; Woolway et al. 2021a, Woolway et al. 2022). Aquatic heatwaves may lower dissolved oxygen (DO) concentrations directly through reduced gas solubility in warmer waters and indirectly through increased ecosystem respiration (Tassone et al. 2021). Low DO concentrations and thermal stress have been linked to coral bleaching, declines in kelp forests, and mass seagrass mortality in marine systems (Wernberg et al. 2016; Hughes et al. 2017; Strydom et al. 2020). Although heatwaves are well-studied in coastal and marine systems, research on the effects of heatwaves in lakes and ponds is relatively nascent (Woolway et al. 2021a; Woolway et al. 2022). As such, it remains unclear how aquatic heatwaves affect the structure and function of lentic ecosystems, especially small, vegetated waterbodies.

Though aquatic heatwaves are projected to be more severe in small, shallow waterbodies (Woolway et al. 2021a), if present, macrophytes may buffer small lakes and ponds from extreme temperatures by restricting vertical heat transfer. Canopy-forming macrophyte beds attenuate incoming solar radiation and dissipate wind-driven turbulence, thus limiting the depth of heat transport and creating a shallow mixed surface layer separated from cooler bottom waters (Herb and Stefan 2004; Andersen et al. 2017a; Sand-Jensen et al. 2019). In short, macrophytes induce thermal stratification in small waterbodies, which may isolate bottom waters from rising surface temperatures during an aquatic heatwave. Stratification is also expected to restrict dissolved gas transport and may produce a vertically heterogenous chemical environment within macrophyte beds (Andersen et al. 2017b; Vilas et al. 2017). As a result, macrophyte structure could also

influence how DO responds to aquatic heatwaves. Rising surface water temperatures during a heatwave are expected to lower DO concentrations; however, in maintaining cooler bottom water temperatures, macrophyte-induced stratification may dampen the effects of a heatwave on gas solubility and DO depletion. Altogether, macrophytes play a key role in the thermal structure and DO environment of small waterbodies, potentially mediating the effect of temporary, external stressors on these ecosystems' structure and function. However, an explicit evaluation of how macrophyte-hydrodynamic interactions may alter ecosystem response to stressors is lacking. This is especially true for lakes and ponds as research on macrophyte-flow interactions has largely focused on coastal and lotic systems (e.g., Fonseca et al. 2019; Tseng and Tinoco 2022).

While macrophytes influence ecosystem structure and function in small waterbodies, environmental conditions also affect macrophytes. The abundance and growth of macrophytes in small waterbodies is driven by temperature and the availability of light and nutrients (Carpenter and Lodge 1986; Phillips et al. 2016), making them sensitive to environmental stressors such as nutrient loading and heatwaves (Wu et al. 2021). Warmer water temperatures can enhance macrophyte growth (Olesen and Madsen 2001, Bertani et al. 2016; Hansson et al. 2020); however, high temperatures may also induce heat stress, impeding reproduction (Li et al. 2017) or prompting senescence (Hao et al. 2018). Similarly, nutrient loading may have either a positive or negative effect on macrophyte growth. Although macrophytes can benefit from enhanced nutrient availability through foliar uptake (DeMarte and Hartman 1974; Twilley et al. 1977), nutrient loading can also increase algal biomass and subsequently reduce light availability through shading (Scheffer et al. 1993; Short et al. 1995). The effect of shading from phytoplankton-associated turbidity is expected to vary across macrophyte growth forms, as submersed species are more vulnerable to light limitation than emergent or floating-leaf species

(Szabo et al. 2010). While the individual responses of macrophytes to nutrient enrichment and heat stress have been established, it remains unclear how macrophytes respond to simultaneous, compounding stressors and what the consequences are for the thermal and chemical structure of small lentic ecosystems.

We experimentally evaluated the interacting effects of episodic external nutrient loading and an extreme heat event on macrophyte biomass and the subsequent changes in the physicochemical environment in two shallow, vegetated ponds. Specifically, we monitored spatiotemporal variation in water column thermal structure, DO profiles, and macrophyte biomass and canopy height in each pond and over the course of a growing season. We experimentally pulsed one of the ponds with nutrients to simulate a typical storm-driven external loading event, while the other pond served as a reference. Both ponds experienced a mid-summer heat event following the first experimental nutrient pulse. In the absence of severe environmental stressors, the phenology of the macrophyte communities in these temperate ponds follows a pattern of spring emergence from over-wintering rhizomes, growth throughout the summer, and then senescence of the leaves and stems in early autumn. However, we hypothesized that the combined stress of the nutrient addition and heat event in the experimentally eutrophied pond would induce early macrophyte senescence due to increased shading from phytoplankton and heat stress, thus reducing macrophyte biomass and subsequently altering the temperature and DO gradients in the water column. To further test the mechanistic relationship between macrophytes and pond hydrodynamics, we applied a hydrodynamic model for one-dimensional heat transport in vegetated ponds and simulated pond response to a heat event across a range of macrophyte biomass and canopy height.

Leveraging our ecosystem experiment and hydrodynamic model, our first research objective was to quantify macrophyte response to the compounding stressors of nutrient enrichment and an extreme heat event as well as the subsequent response of pond thermal structure and DO concentrations. We then explained the observed responses by focusing on the reciprocal relationship between macrophytes and pond hydrodynamics. Specifically, we asked (Q1) How do macrophyte biomass and canopy height influence pond thermal structure, and does macrophyte presence control vertical heat transfer during a heat event? (Q2) How does spatiotemporal variation in DO relate to macrophyte biomass and canopy height, and does macrophyte presence alter the DO response to a heat event? We anticipated that greater macrophyte biomass and canopy height would be associated with stronger thermal stratification and greater differences in DO between surface and bottom waters. We also hypothesized that macrophyte presence would maintain cool water habitat and stable DO concentrations during a heat event. Through the combination of our experiment, observations, and numerical modeling, we found that macrophyte structure can be a source of spatial and seasonal variation in the thermal and chemical environments of shallow waterbodies.

METHODS

Study Site and Field Measurements

We studied how macrophyte structure influences spatiotemporal variation in both the thermal and DO environments of small waterbodies using two ponds at the Iowa State University Horticulture Research Station (42.110005, -93.580454) during the summer of 2020. The ponds are rectangular, relatively small (surface area 400 m^2 at the water line; Figure 1), and shallow (maximum depth 2 m and mean depth 0.8 m), with simple, bowl-shaped bathymetries. These

159 waterbodies fit morphometric and functional definitions of ponds (Richardson et al. 2022). Water
160 balance is driven solely from precipitation and evaporation as there are no surface inflows or
161 outflows and the ponds are lined with bentonite to prevent groundwater interactions. As there is
162 effectively no watershed for these ponds, we effectively controlled all external inputs of
163 nutrients. The ponds were initially filled with water from the research station's irrigation
164 reservoir to seed natural phytoplankton and zooplankton communities. Early in the spring the
165 ponds were stocked with yellow perch (*Perca flavescens*) and bluegill (*Lepomis macrochirus*) at
166 roughly 20 kg ha^{-1} for both species, which is within the range of densities for temperate
167 waterbodies (Carlander 1977; Schneider 1999). The macrophyte community in both ponds was
168 composed of longleaf pond weed (*Potamogeton nodosus*; hereafter "floating-leaf") and leafy
169 pondweed (*Potamogeton foliosus*; hereafter "submerged").
170 External nutrient loading typical of large storm events was simulated by adding nitrogen
171 and phosphorus to one of the ponds (hereafter "nutrient addition pond") twice over the course of
172 the summer. Nitrogen was added as ammonium nitrate (NH_4NO_3), and phosphorus was added as
173 sodium phosphate monobasic dihydrate (($NaH_2PO_4 \bullet (H_2O)_2$) in a ratio of 24N:1P. The first
174 nutrient addition (day of year, DOY, 176) raised the mass of phosphorus in the pond by 3
175 percent, and the second addition (DOY 211) raised the mass by 5 percent. These increases are
176 consistent with the expected nutrient loading from a large storm event in an agricultural
177 landscape (Vanni et al. 2001; Lürling et al. 2018). Nutrients were not added to the other pond
178 (hereafter "reference pond"). To assess and compare the effects of the nutrient additions on algal
179 biomass, we measured chlorophyll-*a* concentrations daily at the deep site of each pond (Figure 1)
180 using the Total Algae sensor as a part of the YSI ProDSS multiparameter sonde (Yellow Springs
181 Instruments, Yellow Springs, Ohio USA). The sensor logged continuously and was slowly

lowered through the water column. Surface concentrations of chlorophyll-*a* were averaged over 0-0.3 m depth in the water column. To minimize drift, the sensor was calibrated regularly against laboratory standards.

To monitor thermal structure and dynamics across the ponds, we deployed vertical strings of high frequency temperature sensors (HOBO 8K Pendant Temperature Data Logger) at three sites, aligned from the deep (2 m) to shallow (1.5 m) ends of each pond (Figure 1). Temperature loggers were distributed throughout the water column every 0.25 m until 1.5 m deep and then every 0.5 to the bottom. Water temperature was logged every 30 minutes from May to August (DOY 143-233). We also took high frequency measurements of surface water DO concentration and saturation at the deep site of both ponds (miniDOT Clear Logger; logging every 30 minutes). In order to quantify the three-dimensional DO environment, manual profiles of DO concentration, DO saturation, and water temperature were taken weekly (13 sampling events total) on a grid of 18 sites across each study pond using a kayak (Figure 1). Measurements were taken in the late morning, between 10:00AM and 12:00PM. A continuous profile of DO was logged at each site as the YSI ProDSS multiparameter sonde was slowly lowered through the water column.

We quantified variation in macrophyte structure over space and time by monitoring community composition, canopy height, and biomass from May to August (DOY 143-233) across the study ponds. Species presence-absence and canopy height were measured weekly at the three sites established from the deep to shallow ends of the ponds (Figure 1). Canopy height was measured as the distance from the sediment-water interface to the top of the canopy. Water depth was also measured at these points so that canopy height could be expressed as a proportion of the water column. Macrophyte dry biomass was sampled every other week (6 sampling events

205 total) on a grid of 18 sites across each pond where manual profiles were also taken (Figure 1).
206 Profiles were always taken before biomass was sampled. To collect a biomass sample, a two-side
207 rake was lowered to the bottom and used to remove submersed and floating-leaf macrophytes
208 from an approximately 0.4 m^2 area (Mikulyuk et al., 2011). All the above-sediment tissue was
209 collected from the rake to determine dry biomass. Samples were dried at 60°C to a constant mass
210 before weighing.
211
212 ***Hydrodynamic Modeling***
213 In order to explore the mechanisms by which changes in macrophyte biomass and canopy
214 height influence pond thermal structure, we applied a one-dimensional hydrodynamic model for
215 vegetated waterbodies. Our model builds upon the one-dimensional, integral energy model by
216 Herb and Stefan (2004) for heat transport in lakes with submersed macrophytes. Macrophytes are
217 incorporated into the model through two key parameters: a light extinction coefficient due to
218 macrophyte biomass shading and a term for turbulent kinetic energy dissipation by macrophytes
219 based on their surface area and drag. Our contributions to the original model include adding
220 convective overturn to address density instabilities over the diurnal cycles, a dynamic
221 macrophyte growth and senescence boundary condition over time, dynamic light attenuation
222 coefficient for water based on daily Secchi depth field data, and coding the model for use
223 through open-source software (R; see Appendix S1 for more details on model algorithms and
224 additional citations).
225 For boundary conditions, the model requires an initial water temperature profile,
226 timeseries of meteorological drivers (air temperature, relative humidity, air pressure, wind speed,
227 and short-wave radiation), and waterbody hypsography (depth-area relationship). We determined

the hypsography of the study ponds through manual calculations based off depth measurements from the profiles taken at 18 sites across each pond. We obtained the necessary meteorological data at an hourly timestep from a weather station located approximately 550 meters from the study ponds and maintained by the Iowa State University Soil Moisture Network (Iowa Environmental Mesonet, ISU Soil Moisture Network 2021). The initial temperature profile was supplied from a single reading from the temperature chain located at the deep site of the reference pond (Figure 1). Macrophyte data were incorporated into the model through weekly measurements of canopy height at the deep site of the reference pond as well as biomass density measurements taken every two weeks. Biomass density standardizes macrophyte biomass to the volume of water sampled ($g\ m^{-3}$). We used the average biomass density from the two sampling sites closest to the deep site temperature sensors, in the southern region of the pond.

The model was run on a 1-hour timestep from late May-August (DOY 143-241; 99 days total). The observed, high frequency water temperature profiles from the deep site of the reference pond were used to calibrate 9 model parameters (Table S1) and assess model fit (quantified as root mean square error, RMSE). Once the model was sufficiently calibrated to the full duration of the observed field data, we manipulated the input macrophyte data to simulate the effect of different macrophyte biomass and canopy dynamics on thermal structure (Table S2). Specifically, we tested a scenario with no macrophytes present in the pond compared to macrophyte biomass and canopy heights that were measured in the reference pond. All modeling analyses were completed in R version 4.1.2 (R Core Team 2021) using the gotmtools (https://github.com/aemon-j/gotmtools), rLakeAnalyzer (Winslow et al. 2019), lubridate (Garrett and Wickham 2011), and tidyverse (Wickham et al. 2019) packages.

Statistical Methods

Our delineation of extreme heat events in the experimental ponds was informed by the definition developed for marine heatwaves (Hobday et al. 2016) and applied more recently to estuaries (Tassone et al. 2021) and lakes (Woolway et al. 2021a). Following this definition, an aquatic heatwave occurs when daily mean surface water temperatures exceed the seasonal 90^{th} percentile threshold for at least 5 days, without dropping below that threshold for 2 or more days. Since we did not have long-term data on summer water temperatures in the experimental ponds, we could not use this formal definition. Therefore, we elected to use temperature monitoring data for the study period only, but a more stringent definition of a heat event threshold (i.e., 95th percentile) for the same extended period (5 days). To determine the 95^{th} percentile surface water temperature for each pond, we used temperature loggers placed at 0 and 0.25 m at the middle at deep sites. For each site, we averaged the readings from these surface loggers, calculated a daily mean, and then averaged values from the middle and deep sites. These steps produced a daily mean surface water temperature for each pond, which we used to calculate the 95^{th} percentile threshold. We then identified any days in which the daily mean surface water temperature exceeded this threshold. A period with at least five days above this threshold was classified as a sustained aquatic heat event (hereafter, "heat event").

To visualize pond thermal structure from our high frequency water temperature data, we used a linear interpolation to estimate temperature for depths at which we either did not place sensors (1.75m deep for both ponds) or for depths at which sensors ceased to function during the summer (1m at the middle and deep sites of the nutrient addition pond, 0.25-0.75m at the shallow site of the nutrient addition pond, and 0.25m at the middle site of the reference pond). The interpolated values were used solely for visualization. Only empirical measurements of

water temperature were used in the model and to calculate indices of pond thermal structure (i.e., thermocline depth and Lake Number). Lake Number is a ratio that compares the internal stability of the water column to external wind stress across the waterbody surface, so it can be used to determine the strength of stratification and likely response to observed wind stress (Robertson et al. 1990). Thermocline depth and Lake Number were calculated using the rLakeAnalyzer package. (Winslow et al. 2019). We defined surface water temperature as the average from the 0 and 0.25m sensors. We used the deepest sensors (2m at the middle and deep sites, 1.5m at the shallow sites) for measurements of bottom water temperature.

In order to compare macrophyte biomass between the study ponds, we calculated the mean macrophyte biomass across 18 sampling sites for each sampling event. However, we weighted this average so that sampling sites around the perimeter of the pond (n=14) had the same weight was sites in the interior or the pond (n=4; Figure 1) so that the mean value would not be biased by water depth. Weighted, pond-averaged macrophyte biomass values were used to plot seasonal changes and explore the relationship between biomass and water column thermal stability. We also standardized macrophyte canopy height as a percent of the water column depth for each sampling site and event to aid comparisons between shallow and deeper sites.

To analyze the manual DO profiles, we first determined that there were no instances of mid-depth DO maximum for any sites or sampling events. The vertical distribution of DO saturation was either uniform, highest in the surface waters, or highest in the bottom waters depending on the site and time of year (Figure S1). Therefore, we focused on DO dynamics in the surface and bottom layers of ponds by averaging values from 0-0.25 m and 0.25 m from the sediment-water interface respectively. Surface and bottom water DO values were used to explore temporal variation, calculate the difference between surface and bottom DO, and quantify

297 variation over space and time. We used coefficients of variation to quantify temporal and spatial
298 variation in surface and bottom water DO saturation. Specifically, spatial variation was defined
299 as the coefficient of variation for DO for each sampling day within each pond, so variation was
300 due to differences among the 18 sampling sites (Figure 1), standardized by the pond-mean for
301 that day. Temporal variation was calculated based on the coefficient of variation in DO for each
302 sampling site, so variation was due to differences in DO over time, standardized by the summer
303 mean DO saturation for that site.
304 A generalized additive model (GAM) was used to smooth the daily time series of
305 chlorophyll concentrations and weekly time series of DO saturation to visually highlight
306 differences in trends over time between the nutrient addition and reference pond. All statistical
307 analyses were completed in R version 4.1.2 (R Core Team 2021) using the mgcv (Wood 2017),
308 rLakeAnalyzer (Winslow et al. 2019), lubridate (Garrett and Wickham 2011), and tidyverse
309 (Wickham et al. 2019) packages.
310
311 **RESULTS**
312 ***Environmental Stressors and Macrophyte Response***
313 Chlorophyll-*a* concentrations were variable in both ponds throughout the experiment, but
314 there was a clear increase in chlorophyll-*a* following the sequential additions of nutrients in the
315 experimental pond (Figure 2A). Early in the season, chlorophyll-*a* concentrations were low in
316 the reference pond, likely due to high *Daphnia sp.* biomass (Butts et al., *in prep*). Following this
317 early clear-water phase and prior to the experimental nutrient additions, chlorophyll-*a*
318 concentrations were similarly low in both ponds (DOY 160). Nutrient additions on DOY 176 and
319 211 resulted in chlorophyll-*a* concentrations 2-3 times higher in the nutrient amended pond

compared to the reference pond. Heightened chlorophyll-*a* concentrations in the nutrient addition pond are indicative of higher algal biomass and thus phytoplankton-associated turbidity, likely resulting in reduced light availability in the nutrient addition pond.

Both ponds experienced a heat event from DOY 185-190 (Figure 2B). During this period, mean daily surface water temperatures exceeded the seasonal 95th percentile in each pond (greater than 29.8 °C in the nutrient addition pond and 30.6 °C in the reference pond). Maximum daily surface water temperatures ranged from 34.5-37.1 °C in the nutrient addition pond and 33.7-38.6 °C in the reference pond during the heat event. Although both ponds had brief periods of high surface water temperatures at other points throughout the summer, DOY 185-190 was the only sustained period of high surface water temperatures ($\geq$ 5 days). The heat event began 9 days after the first nutrient pulse, creating multiple stressors (i.e., reduced light availability and prolonged heat stress) for macrophytes in the nutrient addition pond.

Surface DO saturation was variable over the study period, at times differing between the two study ponds (Figure 2C). Early in the summer, both ponds were supersaturated with DO, and mean surface saturation was similar between the ponds before the initial nutrient addition. In the reference pond, DO remained fairly stable until the heat event (DOY 185-190), after which DO saturation declined and generally remained below saturation for the remainder of the study period. In contrast, mean surface DO saturation in the nutrient addition pond declined immediately following the first nutrient addition (DOY 176) and remained below saturation for the rest of the summer.

Spatiotemporal patterns in macrophyte biomass differed between the ponds and macrophyte growth forms (Figure 2D, 3). The floating-leaf species was largely limited to a ring around the shallower edges of the ponds where the floating leaves could easily reach the surface.

The submerged species was present across a range of depths but reached the highest biomass in the deeper, central region of each pond. In the reference pond, macrophytes followed expected phenology with increasing biomass through late summer and then senescence of both growth forms beginning in early autumn (Figure 2D, 3). The heat event did not affect macrophyte biomass or assembly in the reference pond. However, in the nutrient addition pond, submerged macrophytes growing in 1.75 to 2 m of water began to senesce following the initial nutrient addition and heat event such that no plants were present in the deepest areas of the nutrient addition pond 9 days (DOY 199) after the heat event and the middle site of the pond 23 days (DOY 213) after the heat event ended (Figure 3). Early senescence of submersed macrophytes in the nutrient addition pond resulted in rapid declines in both biomass (Figure 2D) and canopy height (Figure 4). Both submersed and floating-leaf plants persisted in shallow water around the edge of the pond through the end of the summer.

Spatiotemporal Variation in Pond Thermal Structure

Both ponds experienced intermittent thermal stratification during the study period and similar spatial patterns of stratification from shallow to deep ends of the pond (Figure 4). Early in the summer, both ponds were cool and isothermal. As surface waters began to warm, the middle and deep sites of both ponds began to stratify while the shallow sites remained fairly well-mixed. At the center of the ponds, a stable thermocline between 1-1.5 m depth was observed in the reference pond between DOY 155-161, and almost constantly between DOY 168-210 (Figure S2A), while the thermocline in the nutrient addition pond was more intermittent (DOY 157-159, 170-174, and 178-192; Figure S2B). When present, pond thermoclines cooled and deepened slightly (0.05-0.1 m) during the night, indicating nighttime convective cooling and

366 mixing in the surface layer. During periods of thermal stratification, differences between surface
367 and bottom water temperatures ranged from 4.3 to 11.5 °C (mean 8.1°C) in the reference pond
368 and 4.5 to 10.2 °C (mean 7.3 °C) in the nutrient addition pond.

369 Similarities in pond thermal structure occurred during times of similar macrophyte
370 coverage, either early or late in the season (Figure 4). For example, both ponds experienced a
371 strong mixing event in late summer (DOY 216-220), driven by cooler air temperatures and
372 higher wind speeds (Figure 5) and facilitated by declining macrophyte structure (Figure 4).
373 Similar meteorological conditions occurred earlier in the summer and resulted in some water
374 cooling (e.g., DOY 164, 175); however, the ponds did not mix as fully during these events, likely
375 due to the macrophyte structure present in both ponds in early summer (Figure 4). Similarities in
376 pond thermal structure in relation to extrinsic factors (i.e., wind speed) are further demonstrated
377 by similar lake number values for both ponds over the study period (Figure S3).

378 Although overall seasonal patterns in thermal structure were similar between the ponds,
379 there were brief dissimilarities, related to differences in the timing of macrophyte senescence
380 (Figure 4). There was a prolonged period of stable thermal stratification from DOY 180-210 in
381 the reference pond, with only brief instability between DOY 198-199. A stable thermocline set-
382 up in the nutrient addition pond around the same time (DOY 178); however, stratification began
383 to break down approximately 18 days earlier (DOY 192) than in the reference pond (Figure S2).
384 The timing of destratification in the nutrient addition pond coincides with declines in macrophyte
385 biomass (Figure 3) and canopy height (Figure 4) in the center of the pond. Destratification in the
386 reference pond also followed patterns of biomass senescence and loss of canopy height, although
387 this did not occur until later in the summer in this pond. In both ponds, there was strong temporal
388 coherence between the timing of destratification and macrophyte senescence, driven by the

compounding stress of eutrophication and a heat event in the nutrient addition pond and typical seasonal senescence in the reference pond. The declines in canopy cover and biomass were associated with increased thermal mixing and warmer bottom water temperatures, especially in the nutrient addition pond.

During the aquatic heat event (DOY 185-190), both ponds experienced a similar increase in surface water temperatures (Figure 2B, Figure 4). However, there was a stark difference in the response of bottom water temperatures at the deep and middle sites between the ponds (Figure S4). During the heat event, bottom water temperature remained consistent at both the deep and middle sites of the reference pond. The daily mean bottom water temperature increased by only 0.2 °C at both sites. In contrast, bottom water temperatures in the nutrient addition pond did respond to the heat event, increasing by 1.3 °C and 1.4 °C at the deep and middle sites, respectively. At the shallow site in both ponds bottom water temperatures increased 1-1.3 °C during the heat event, suggesting an interaction with water depth. The different response of bottom water temperature to the heat event related to differences in macrophyte biomass between the two ponds. At the time of the heat event, macrophyte biomass (Figure 2D) and canopy height (Figure 4) were greater in the reference pond because submersed macrophytes in the center of the nutrient addition pond began to senesce following the first nutrient pulse (DOY 176; Figure 3). Overall, bottom waters in the nutrient addition pond warmed over the course of the heatwave while cooler bottom water temperatures were maintained in the reference pond, despite significant warming in the surface layers.

Spatiotemporal Variation in Dissolved Oxygen

In both ponds, DO varied across sites, vertically in the water column, and over time. Weekly DO profiles captured broad seasonal trends in surface DO saturation as similar temporal patterns were observed between weekly and high-frequency values (Figure 2C, S5A). Surface waters were supersaturated with DO early in the summer in both ponds (Figure S5A). In the reference pond, mean pond surface DO declined through DOY 170, remained fairly stable, and then declined again during the heat event (DOY 185-190). In the nutrient addition pond, surface DO saturation was similar to the reference pond before the nutrient addition. Surface DO then decreased after the nutrient addition and through the heat event. Over a one-week period during and after the heat event (DOY 186-192), DO saturation fell 22.4% and 50.4% in the nutrient addition and reference ponds, respectively. After the heat event, surface DO in both ponds was generally below saturation, with increased instances of DO saturation below 25%. Bottom water DO saturation mirrored the seasonal pattern in surface DO (Figure S5B). For both ponds the difference in DO saturation between surface and bottom waters was most pronounced early in the season (reference pond range -87.1 to 23.3%; nutrient addition pond range -56.8 to 58.8%). Surface and bottom water DO saturation became more similar throughout the summer, especially following the heat event (reference pond range -2.1 to 17.0%; nutrient addition pond range -0.3 to 12.2%; Figure S5C).

For both surface and bottom water DO saturation, temporal variation on a seasonal scale was greater than spatial variation across the ponds (Table 1). The coefficient of variation at a given site in the pond over time was 3.6-5.2 times greater than the variation among sites on a given sampling day. The magnitude of temporal versus spatial variation was similar between ponds. Seasonal patterns in DO saturation followed some trends with declining macrophyte

biomass following the nutrient addition associated with lower DO; however, the heat event had the most pronounced effect on seasonal DO patterns (Figure 6).

Mechanisms of Macrophyte Control of Pond Hydrodynamics

We used a one-dimensional hydrodynamic model to illuminate the mechanistic relationship between macrophytes and pond thermal structure and test how macrophyte presence mediates the degree to which bottom water temperatures warm in response to a heat event. We based our model on the deep site of the reference pond. The model projections were consistent with the observed temperature profiles (mean RMSE 1.67 °C across 8 discrete depths; Figure S6). Error was greatest in the surface waters (0 m; RMSE 2.47 °C), where the model underpredicted water temperature and did not capture the full range of observed diel oscillations, especially early in the summer. Error was lower in the bottom waters of the pond (1.25-2 m). The model underpredicted water temperature early in the summer but then showed good agreement with the observed temperatures (RMSE range 1.05-1.52 °C). Overall, the model captured the magnitude and seasonal trends of temperature throughout the water column.

We applied the hydrodynamic model to quantify differences in pond thermal structure under contrasting scenarios of macrophyte presence (Figure 7). Specifically, we tested a scenario in which there were no macrophytes present (i.e., canopy height and biomass density were set to zero over the study period) and compared the results to the model output for the reference pond when the observed macrophyte data were used (Table S2). Under the scenario where macrophytes were present, the model predicted strong stratification during the period of peak macrophyte biomass and canopy height in the middle of the summer and cool bottom water temperatures throughout the study period (Figure 7A). In contrast, under the scenario in which

456 macrophytes were entirely absent from the pond, the model predicted complete water column
457 mixing and much warmer temperatures throughout the water column, especially following the
458 aquatic heat event (Figure 7B). When macrophytes were present, the increase in bottom water
459 temperatures over the course of the aquatic heat event was negligible (0.01 °C), and bottom
460 temperatures then remained below 25 °C for the remainder of the summer (maximum
461 temperature 23.3 °C; Figure 7A, C). However, the no-macrophyte scenario resulted in a 1.92 °C
462 increase in bottom water temperatures during the heat event and much higher maximum water
463 temperatures later in the summer (33.4 °C; Figure 7B, C). The model simulations demonstrate
464 that macrophyte structure increases thermal stratification and promotes cooler bottom water
465 temperatures, even during an extreme heat event.
466
467 **DISCUSSION**
468 We leveraged an ecosystem experiment and complimentary hydrodynamic model to test
469 macrophyte response to compounding stressors (i.e., stochastic external nutrient loading and
470 extreme heat events) and evaluate the consequences of stress-induced macrophyte senescence for
471 the physicochemical environment in two shallow, vegetated ponds. The type and severity of
472 environmental stressors differed between the study ponds, producing distinct temporal patterns in
473 macrophyte assembly and coverage. In the reference pond, both submersed and floating-leaf
474 macrophytes followed the expected phenology of spring emergence, summer growth, and then
475 senescence beginning in late summer. This natural phenology may be attributed to the lack of
476 severe physiological stressors in the reference pond. Although this pond did experience a heat
477 event, dense macrophyte beds limited the depth of water column warming and maintained stable
478 bottom water temperatures. In contrast, submersed macrophytes in the nutrient addition pond

479 began to senesce in mid-summer after the first experimental nutrient pulse and continuing after
480 the heat event. This early senescence was dominated by submersed macrophytes in the deeper,
481 central region of pond, suggesting that light limitation from phytoplankton shading was a
482 contributing stressor (Scheffer et al. 1993; Short et al. 1995; Phillips et al. 2016). Light limitation
483 may have been exacerbated by heat stress, which was likely more acute in the nutrient addition
484 pond as declining macrophyte biomass following the nutrient pulse allowed temperatures to rise
485 throughout the water column rather than just the surface layers. Early senescence of submersed
486 macrophytes in the nutrient addition pond as a result of compounding stressors altered the
487 thermal environment and DO saturation in relation to the reference pond.
488
489 ***Thermal Structure***
490 On a seasonal scale, we observed strong temporal coherence between macrophyte growth
491 and senescence and pond thermal structure. Both ponds began to experience intermittent thermal
492 stratification in early summer, once macrophytes had grown to fill the majority of the water
493 column. This threshold is consistent with the expectation that canopy-forming macrophyte beds
494 may induce diurnal stratification once they occupy at least 50 percent of the water column (Vilas
495 et al. 2017). By mid-summer we observed strong thermal stratification, characterized by large
496 differences (around 10°C) between surface and bottom water temperatures, comparable to
497 stratification in other small, vegetated ponds (Andersen et al. 2017a; Vilas et al. 2017). However,
498 in other studies, macrophyte-induced stratification followed diel cycles, with daytime
499 stratification and nighttime overturn due to convective mixing (Martinsen et al. 2019; Sand-
500 Jensen et al. 2019), which can move through macrophyte structure more readily than external
501 turbulent mixing (Herb and Stefan 2005; Andersen et al. 2017b). Although we observed

nighttime convective cooling and mixing in the surface of the ponds during periods of macrophyte-induced stratification, convective cooling did not mix the entire water column. Stable thermal stratification began to break down in both study ponds during macrophyte senescence. Declining macrophyte canopy height and biomass removed structural barriers that had previously attenuated incoming solar radiation and dissipated wind-driven turbulent mixing (Herb and Stefan 2004), allowing the warm, mixed surface layer to deepen and eventually mix the entire water column. However, the timing of both destratification and macrophyte senescence differed between the study ponds, driven by compounding stressors in the nutrient addition pond and typical seasonal senescence in the reference pond. In the nutrient addition pond consistent water column mixing began when macrophyte biomass and canopy height in the center of the pond began to decline in response to phytoplankton-shading following the experimental nutrient pulse and the heat event.

Macrophyte presence mediated how pond thermal structure responded to an extreme heat event by restricting vertical heat transfer and maintaining cooler bottom water temperatures. Both study ponds saw high surface water temperatures during the heat event. However, as anticipated, the depth of water column warming and overall change in bottom water temperature differed between the ponds as a result of differences in macrophyte coverage. At the time of the heat event, macrophyte canopy height and biomass were rapidly declining in center of the nutrient addition pond due to phytoplankton-shading. In the reference pond, macrophyte biomass was still increasing and the canopy reached to fill over 75 percent of the water column. During the heat event, a layer of cooler water between 0.25 and 0.5 m thick remained in the reference pond, with only subtle increases in daily mean temperature (+0.2 °C). In contrast, the nutrient addition pond saw increasing water temperatures throughout the water column, including a 1.3°C

525 increase in daily mean temperatures in the deepest waters of the pond over the 5-day heat event.
526 Given the observed differences between the study ponds, it is very likely that macrophyte
527 structure played a pivotal role in mediating the depth and degree of water column warming
528 during the aquatic heat event. Nevertheless, thermal structure in small waterbodies arises from
529 complex interactions between waterbody features and external forces (Herb and Stefan 2004;
530 Branco and Torgersen 2009). In order to explicitly test the mechanisms underpinning the
531 differences we saw between the study ponds and evaluate the role of macrophytes, we used a
532 hydrodynamic model for heat transport in vegetated waterbodies and simulated water column
533 thermal structure during a heat event under contrasting scenarios of macrophyte density.
534 The model results support our field observations and demonstrate that macrophytes
535 structure the thermal environment in shallow ponds through vertical attenuation of both light and
536 turbulent kinetic energy. Simulations of seasonal patterns in pond thermal structure under
537 variable macrophyte density revealed that macrophyte presence reduces the depth and degree of
538 water column warming both during and after an aquatic heat event and maintains cooler bottom
539 water temperatures throughout the course of the summer. Our experimental observations and
540 model simulations provide evidence that macrophytes may buffer small waterbodies from brief
541 aquatic heatwaves, at least with the vertical extent of warming in the water column. As aquatic
542 heatwaves become more widespread and frequent, heatwaves in small waterbodies are expected
543 to be shorter but more intense compared to larger waters (i.e., due to lower thermal inertia;
544 Woolway et al. 2021a; Polazzo et al. 2021; Woolway et al. 2022). Our findings suggest that
545 macrophytes can mediate the intensity of brief aquatic heatwaves in small lakes and ponds. As
546 such, managing for robust macrophyte communities is a potential tool for mitigating heatwave

547 effects in small waterbodies and promoting thermal heterogeneity to support other aquatic
548 organisms (Carpenter and Lodge 1986; Till et al. 2019).
549 Our hydrodynamic model enhances a conceptual and analytical framework for
550 incorporating biological structure into one-dimensional heat transport models (Herb and Stefan
551 2004). Overall, there was good agreement between the model predications and the observed
552 temperature profiles. The largest discrepancies between the model output and field data occurred
553 in early summer when the model underpredicted temperature. The early summer period
554 coincides with rapid growth in macrophyte biomass and canopy height. It is possible that the
555 temporal resolution of our field data during this time was insufficient to accurately capture
556 biological dynamics in the pond for the model input. Canopy height was measured weekly while
557 biomass was collected every two weeks. More frequent observations could have fit the
558 macrophyte input data closer to conditions captured by the high frequency temperature profiles.
559 Additionally, other one-dimensional heat transport models (i.e., Simstrat, GOTM, GLM) have
560 been shown to have greater error during extreme meteorological events, including atmospheric
561 heatwaves (Mesman et al. 2020). This tendency could explain some of the disparities between
562 model output and field data during a brief period of high air temperatures around DOY 155,
563 reflected in rapid increases in water temperature in the first 1.25 m of the profile. Our model
564 would benefit from additional testing across a variety of vegetated waterbodies to inform best
565 practices for applying this approach in other waters. However, our findings indicate that
566 macrophytes should be incorporated into hydrodynamic models for vegetated systems, and our
567 modeling approach provides an example of how to do so.
568
569 ***Dissolved Oxygen***

570 Within both study ponds, DO saturation varied on a seasonal scale and responded to the
571 experimental nutrient pulse as well as the heat event. We had anticipated greater spatial variation
572 in DO saturation within each pond as a result of macrophyte-induced thermal stratification. This
573 expectation was based on evidence of steep vertical gradients of DO and dissolved inorganic
574 carbon in other shallow, vegetated waterbodies (Andersen et al. 2017a; Vilas et al. 2017).
575 However, most of the DO profiles were uniform with depth, suggesting that the balance of
576 processes releasing and consuming oxygen (e.g., gross primary production versus respiration)
577 were similar throughout the ponds or that DO was able to diffuse readily throughout the water
578 column. Temporal patterns in surface and bottom water DO saturation were connected to the
579 compounding environmental stressors, beginning with the initial experimental nutrient addition.
580 Following the first nutrient pulse, DO remained stable in the reference pond but declined below
581 100 percent saturation in the experimental pond. We might have expected to see increased DO
582 after the nutrient addition as a result of enhanced phytoplankton production, but the observed
583 decline in DO suggests that ecosystem respiration was stimulated by the added nutrients,
584 outweighing any increases in gross primary production. Stress-induced macrophyte senescence
585 likely contributed to this pattern through reduced macrophyte photosynthesis and dramatic
586 increases in macrophyte necromass, the decomposition of which would consume oxygen.
587 Although we observed differences in DO saturation between the ponds after the nutrient
588 addition, the most pronounced temporal shift in DO occurring following the heat event.
589 During the heat event, DO saturation feel sharply in both ponds and remained depressed
590 through the remainder of the study period. We had expected macrophyte structure to maintain
591 stable DO saturation in the bottom waters of the reference pond; however, both ponds responded
592 similarly, regardless of the differences in macrophyte coverage and thermal structure. Our

observations support findings from freshwater and marine systems that aquatic heatwaves are associated with declines in DO due to reduced gas solubility and increased respiration rates (Ali et al. 2016; Brauko et al. 2020; Tassone et al. 2021). Reduced DO availability has consequences for nutrient and carbon cycling as well as greenhouse gas production. For example, anoxia within the sediment profile can mobilize phosphorus from redox-sensitive minerals (i.e., anaerobic internal phosphorus loading; Orihel et al. 2017). Anoxic conditions in the sediments also promote denitrification and methanogenesis, two microbial processes that can produce potent greenhouse gases (i.e., nitrous oxide and methane respectively; Fonseca et al. 2017; Ming et al. 2022). Both denitrification and methanogenesis require organic carbon substrate, which was augmented by macrophyte necromass in the nutrient addition pond (Boon et al. 1995; Bastviken et al. 2005; Deng et al. 2020). Although both ponds likely experienced shifts in other elemental cycles as a result of reduced DO saturation during the aquatic heatwave, the consequences for greenhouse gas production were likely more pronounced in the nutrient addition pond due to early macrophyte senescence increasing organic matter inputs to the sediments. This difference between the study ponds highlights the complex interactions that may arise from compounding stressors in lentic ecosystems.

Conclusions

Aquatic heatwaves are becoming more frequent and are likely to co-occur with chlorophyll-*a* maxima in lakes and ponds (i.e., algal blooms; Woolway et al. 2021b). As such, there is a growing need to understand and forecast how lentic ecosystems will respond to compound, extreme events. Our findings illuminate the role that macrophyte-hydrodynamic interactions play in mediating ecosystem response to multiple stressors. Overall, dense

macrophyte structure can buffer small waterbodies from brief aquatic heat events by restricting vertical heat transport. However, declines in DO saturation are expected during heat events, regardless of macrophyte coverage. Our findings also reinforce that small lakes and ponds are vulnerable to nutrient loading and temperature extremes. Given the prevalence and importance of small waterbodies for biodiversity and biogeochemical processing, it is essential that we continue to build our mechanistic understanding of the effects of compound, extreme events in these ecosystems and the role that macrophytes can play in ameliorating stressors.

Acknowledgements

Albright was supported by the National Science Foundation (NSF) Graduate Research Fellowship Program (DGE-1747503). Additional Support was also provided by the Graduate School and the Office of the Vice Chancellor for Research and Graduate Education at the University of Wisconsin-Madison with funding from the Wisconsin Alumni Research Foundation. Wilkinson was supported by the NSF Division of Environmental Biology (1942256 and 2200391). Ladwig was supported by the NSF Harnessing the Data Revolution grant (1934633), the University of Wisconsin-Madison Data Science Initiative, and the NSF Advances in Biological Informatics development grant (DBI 1759865). Any opinions, findings, and conclusions or recommendations expressed in this material are those of the authors and do not necessarily reflect the views of the National Science Foundation. Thank you to Tyler Butts, Matthew Kots, Michael Tarnow, and Robert Johnson for collection and use of ancillary data sets.

Data Availability Statement

The data supporting the conclusions and the analysis code are available in the Github repository https://github.com/AlbrightE/pond_physics_2022. Following manuscript acceptance, the Github

repository will be archived on Zenodo, and the data will be published on the Environmental Data Initiative's online repository under a Creative Commons Attribution license (CC-BY).

REFERENCES

1. Ali, S., P.K. Mishra, A. Islam, and N.M. Alam. 2016. Simulation of water temperature in a small pond using parametric statistical models: Implications of climate warming. J. Environ. Eng. 143(3): 04015085, doi: 10.1061/(ASCE)EE.1943-7870.0001050

2. Andersen, M.R., T. Kragh, and K. Sand-Jensen. 2017a. Extreme diel dissolved oxygen and carbon cycles in shallow vegetated lakes. Proc. Biol. Sci. 284: 20171427, doi: 10.1098/rspb.2017.1427

3. Andersen, M.R., K. Sand-Jensen, R.I. Woolway, I.D. and Jones. 2017b. Profound daily vertical stratification and mixing in a small, shallow, wind-exposed lake with submerged macrophytes. Aquat. Sci. 79: 395-406, doi: 10.1007/s00027-016-0505-0

4. Bastviken, S.K., P.G. Eriksson, A. Premrov, and K. Tonderski. 2005. Potential denitrification in wetland sediments with different plant species detritus. Ecol. Eng. 24(2): 183-190, doi: 10.1016/j.ecoleng.2005.04.013

5. Battin, T. J., S. Luyssaert, L.A. Kaplan, A.K. Aufdenkampe, A. Richter, and L.J. Tranvik. 2009. The boundless carbon cycle. Nat. Geosci. 2: 598-600, doi: 10.1038/ngeo618

6. Bertani, I., R. Primicerio., and G. Rossetti. 2016. Extreme climatic event triggers a lake regime shift that propagates across multiple trophic levels. Ecosystems. 19(1): 16–31, doi:10.1007/s10021-015-9914-5

7. Biggs, J., S. von Fumetti, and M. Kelly-Quinn. 2017. The importance of small waterbodies for biodiversity and ecosystem services: implications for policy makers. Hydrobiologia. 793: 3-39, doi: 10.1007/s10750-016-3007-0

8. Boon, P.I., and A. Mitchell. 1995. Methanogenesis in the sediments of an Australian freshwater wetland: Comparison with aerobic decay, and factors controlling methanogenesis. FEMS Microbiol. Ecol. 18(3): 175-190, doi: 10.1016/0168-6496(95)00053-5

9. Borchers, H.W. 2021. adagio: Discrete and Global Optimization Routines. R package version 0.8.4. https://CRAN.R-project.org/package=adagio

10. Branco, B.F., and T. Torgersen. 2009. Predicting the onset of thermal stratification in shallow inland waterbodies. 71(1): 65-79, doi: 10.1007/s00027-009-8063-3

11. Brauko, K.M., and others. 2020. Marine Heatwaves, Sewage and Eutrophication Combine to Trigger Deoxygenation and Biodiversity Loss: A SW Atlantic Case Study. Front. Mar. Sci. 7, doi: 10.3389/fmars.2020.590258

12. Carlander, K.D. 1977. Biomass, Production, and Yields of Walleye (Stizostedion vitreum vitreum) and Yellow Perch (Perca flavescens) in North American Lakes. J. Fish. Res. Board Can. 34(10): 1602-1612, doi: 10.1139/f77-225

13. Carpenter, S.R., and D.M. Lodge. 1986. Effects of submersed macrophytes on ecosystem processes. Aquat. Bot. 26: 341-370, doi: 10.1016/0304-3770(86)90031-8

14. Cole, J.J., and others. 2007. Plumbing the global carbon cycle: Integrating inland waters into the terrestrial carbon budget. Ecosystems. 10(1): 171-184, doi: 10.1007/s10021-006-9013-8

15. DeMarte, J.A., and R.T. Hartman. 1974. Studies of Absorption of ^{32}P, ^{59}Fe, and ^{45}Ca by Water-Milfoil (Myriophyllum Exalbescens Fernald). Ecology, 55(1): 188-194, doi: 10.2307/1934635

16. Deng, H.G., J. Zhang, J.J. Wu, X. Yao, and L.W. Yang. 2020. Biological denitrification in a macrophytic lake: implications for macrophytes-dominated lake management in the north of China. Environ. Sci. Pollut. Res. 27(34): 42460-42471, doi: 10.1007/s11356-020-10230-3

17. Downing, J. 2010. Emerging global role of small lakes and ponds: little things mean a lot. Limnetica. 29(10): 9-24.

18. Fonseca, A.L.D., C.C. Marinho, and F.D. Esteves. 2017. Potential methane production associated with aquatic macrophytes detritus in a tropical coastal lagoon. Wetlands. 37(4): 763-771, doi: 10.1007/s13157-017-0912-6

19. Fonseca, M.S., J.W. Fourqurean, and M.A.R. Koehl. 2019. Effect of seagrass on current speed: Importance of flexibility vs. shoot density. Front. Mar. Sci. 6: 376, doi: 10.3389/fmars.2019.00376

20. Hao, B., A.F. Roejkjaer, H. Wu, Y. Cao, E. Jeppesen, and W. Li. 2018. Responses of primary producers in shallow lakes to elevated temperature: a mesocosm experiment during the growing season of Potamogeton crispus. Aquat. Sci. 80: 34, doi: 10.1007/s00027-018-0585-0

21. Hansson, L.-A., M.K. Ekvall., L. He, Z. Li, M. Svensson, P. Urrutia-Cordero, and H. Zhang. 2020. Different climate scenarios alter dominance patterns among aquatic primary producers in temperate systems. Limnol. Oceanogr. 65(10): 2328–2336, doi:10.1002/lno.11455

22. Herb, W.R., and H.G. Stefan. 2004. Temperature stratification and mixing dynamics in a shallow lake with submersed macrophytes. Lake Reserv. Manag. 20(4): 296-308, doi: 10.1080/07438140409354159

23. Herb, W.R., and H.G. Stefan. 2005. Model for Wind-Driven Vertical Mixing in a Shallow Lake with Submersed Macrophytes. J. Hydraul. Eng. 131(6): 488-496, doi: 10.1061/(ASCE)0733-9429(2005)131:6(488)

24. Hobday, A.J., and others. 2016. A hierarchical approach to defining marine heatwaves. Prog. Oceanogr. 141: 227-238, doi: 10.1016/j.pocean.2015.12.014

25. Holgerson, M.A., and P. A. Raymond. 2016. Large contribution to inland water CO_2 and CH_4 emissions from very small ponds. Nat. Geosci. 9: 222-226, doi: 10.1038/ngeo2654

26. Hughes, T.P., and others. 2017. Global warming and recurrent mass bleaching of corals. Nature. 543: 373-377, doi: 10.1038/nature21707

27. Iowa Environmental Mesonet. 2020. Iowa State University Soil Moisture Network. https://mesonet.agron.iastate.edu/agclimate/hist/hourly.php. Accessed 15 November 2021.

28. Li, Z., L. He, H. Zhang, P. Urrutia-Cordero, M.K. Ekvall, J. Hollander, and L.-A. Hansson. 2017. Climate warming and heat waves affect reproductive strategies and interactions between submerged macrophytes. Glob. Chang. Biol. 23: 108–116, doi: 10.1111/gcb.13405

29. Licci, S., H. Nepf, C. Delolme, P. Marmonier, T.J. Bouma, and S. Puijalon. 2019. The role of patch size in ecosystem engineering capacity: a case study of aquatic vegetation. Aquat. Sci. 81(3), doi: 10.1007/s00027-019-0635-2.

30. Lürling, M., M. M. Mello, F. van Oosterhout, L. de S. Domis, and M. M. Marinho. 2018. Response of natural cyanobacteria and algae assemblages to a nutrient pulse and elevated temperature. Front. Microbiol. 9: 1–14, doi:10.3389/fmicb.2018.01851

31. Martinsen, K.T., M.R. Andersen, and K. Sand-Jensen. 2019. Water temperature dynamics and the prevalence of daytime stratification in small temperate shallow lakes. Hydrobiologia. 826: 247–262, doi:10.1007/s10750-018-3737-2

32. Mesman, J.P., and others. 2020. Performance of one-dimensional hydrodynamic lake models during short-term extreme weather events. Environ. Modell. Softw. 133: 104852, doi: 10.1016/j.envsoft.2020.104852

33. Messager, M.L., B. Lehner, G. Grill, I. Nedeva, and O. Schmitt. 2016. Estimating the volume and age of water stored in global lakes using a geo-statistical approach. Nat. Comm., 7: 13603, doi: 10.1038/ncomms13603

34. Ming, N., X. Liang, L.J. Hou, W.P. Li, and C.Q. He. 2022. Submerged macrophytes regulate diurnal nitrous oxide emissions from a shallow eutrophic lake: A case study of Lake Wuliangsuhai in the temperate arid region of China. Sci. Total. Environ. 811: 152451, doi: 10.1016/j.scitotenv.2021.152451

35. Olesen, B., and T.V. Madsen. 2001. Growth and physiological acclimation to temperature and inorganic carbon availability by two submerged aquatic macrophyte species, Callitriche cophocarpa and Elodea canadensis. Funct. Ecol. 14(2): 252-260, doi: 10.1046/j.1365-2435.2000.00412.x

36. Oliver, E.C.J., and others. 2018. Longer and more frequent marine heatwaves over the past century. Nat. Commun. 9, 1324, doi:10.1038/s41467-018-03732-9

37. Orihel, D.M., H.M. Baulch, N.J. Casson, R.L. North, C.T. Parsons, D.C.M Seckar, and J.J. Venkiteswaran. 2017. Internal phosphorus loading in Canadian fresh waters: a critical review and data analysis. Can. J. Fish. Aquat. Sci. 74: 2005-2029, doi: 10.1139/cjfas-2016-0500

38. Peacock, M., and others. 2021. Small artificial waterbodies are widespread and persistent emitters of methane and carbon dioxide. Glob. Chang. Biol. 27(20): 5109-5123, doi: 10.1111/gcb.15762

39. Phillips, G., N. Willby, and B. Moss. 2016. Submerged macrophyte decline in shallow lakes: What have we learnt in the last forty years? Aquat. Bot. 135: 37-45, doi: 10.1016/j.aquabot.2016.04.004

40. Polazzo, F., S.K. Roth, M. Hermann, A. Mangold-Döring, A. Rico, A. Sobek, P.J. Van den Brink, M.C. Jackson. 2022. Combined effects of heatwaves and micropollutants on freshwater ecosystems: Towards an integrated assessment of extreme events in multiple stressors research. Glob. Chang. Biol. 28: 1248-1267, doi 10.1111/gcb.15971

41. Richardson, D.C., and others. 2022. A functional definition to distinguish ponds from lakes and wetlands. Sci. Rep. 12: 10472, doi: 10.1038/s41598-022-14569-0

42. Robertson, D.M., J. Imberger, and K. Boland. 1990. Lake Number: A quantitative indicator of mixing to be used in water quality management. Water: J. Australian Water and Wastewater Assoc. Dec.: 29-33.

43. Sand-Jensen, K., M.R. Andersen, K.T. Martinsen, J. Borum, E. Kristensen, and T. Kragh. 2019. Shallow plant-dominated lakes – extreme environmental variability, carbon cycling and ecological species challenges. Ann. Bot. 124: 35-366. doi: 10.1093/aob/mcz084.

44. Scheffer, M., and others. 2006. Small habitat size and isolation can promote species richness: second-order effects on biodiversity in shallow lakes and ponds. Oikos. 112(1): 227-231, doi:10.1111/j.0030-1299.2006.14145.x

45. Scheffer, M., S.H. Hosper, M.L. Meijer, B. Moss, and E. Jeppesen. 1993. Alternative equilibria in shallow lakes. Trends. Ecol. Evol. 8 (8): 275-279, doi: 10.1016/0169-5347(93)90254-M

46. Schneider, J.C. 1999. Dynamics of quality bluegill populations in two Michigan lakes with dense vegetation. N. Am. J. Fish. Manage. 19(1): 97-109, doi: 10.1577/1548-8675(1999)019<0097:DOQBPI>2.0.CO;2

47. Short, F.T., D.M. Burdick, and J.E. Kaldy III. 1995. Mesocosm experiments quantify the effects of eutrophication on eelgrass, Zostera marina. Limnol. Oceanogr. 40(4): 740-749, doi: 10.4319/lo.1995.40.4.0740

48. Strydom, S., and others. 2020. Too hot to handle: Unprecedented seagrass death driven by marine heatwave in a World Heritage Area. Glob. Change. Biol. 26(6): 3525-3538, doi: 10.1111/gcb.15065

49. Szabo, S., M. Scheffer, R. Roijackers, B. Waluto, M. Braun, P.T. Nagy, G. Borics, and L. Zambrano. 2010. Strong growth limitation of a floating plant (Lemna gibba) by the submerged macrophyte (Elodea nuttallii) under laboratory conditions. Freshwater. Biol. 55(3): 681-690, doi: 10.1111/j.1365-2427.2009.02308.x

50. Tassone, S.J., A.F. Besterman, C.D. Buelo, J.A. Walter, and M.L. Pace. 2021. Co-occurrence of Aquatic Heatwaves with Atmospheric Heatwaves, Low Dissolved Oxygen, and Low pH Events in Estuarine Ecosystems. Estuar. Coast. 45: 707-720, doi:10.1007/s12237-021-01009-x

51. Taylor, S., P.J. Gilbert, D.A. Cooke, M.E. Deary, and M.J. Jeffries. 2019. High carbon burial rates by small ponds in the landscape. Front. Ecol. Environ. 17(1): 25-31, doi: 10.1002/fee.1988

52. Till, A., A.L. Rypel, A. Bray, and S.B. Fey. 2019. Fish die-offs are concurrent with thermal extremes in north temperate lakes. Nat. Clim. Chang. 9, 637–641, doi: 10.1038/s41558-019-0520-y

53. Tseng, C.Y., and R.O. Tinoco. 2022. From substrate to surface: A turbulence-based model for gas transfer across sediment-water-air interfaces in vegetated streams. Water Resour. Res. 58(1): e2021WR030776, doi: 10.1029/2021WR030776

54. Twilley, R.R., M.M., Brinson, and G.J. Davis. 1977. Phosphorus absorption, translocation, and secretion in Nuphar luteum. Limnol. Oceanogr. 22(6): 1022-1032, doi: 10.4319/lo.1977.22.6.1022

55. Van Geest, G.J., F.C.J.M. Roozen, H. Coops, R.M.M. Roijackers, A.D. Buijse, E.T.H.M. Peeters, and M. Scheffer. 2003. Vegetation abundance in lowland flood plan lakes determined by surface area, age and connectivity. Freshw. Biol. 48(3): 440-454, doi: 10.1046/j.1365-2427.2003.01022.x

56. Vanni, M. J., W. H. Renwick, J. L. Headworth, J. D. Auch, and M. H. Schaus. 2001. Dissolved and particulate nutrient flux from three adjacent agricultural watersheds: A five-year study. Biogeochemistry 54: 85–114, doi:10.1023/A:1010681229460

57. Vilas, M.P, C.L. Marti, M.P. Adams, C.E. Oldham, and M.R. Hipsey. 2017. Invasive macrophytes control the spatial and temporal patterns of temperature and dissolved oxygen in a shallow lake: A proposed feedback mechanism of macrophyte loss. Front. Plant. Sci. 8: 2097. doi: 10.3389/fpls.2017.02097.

58. Wilkinson, G.M., A. Besterman, C. Buelo, J. Gephart, and M.L. Pace. 2018. A synthesis of modern organic carbon accumulation rates in coastal and aquatic inland ecosystems. Sci. Rep. 8: 15736, doi: 10.1038/s41598-018-34126-y

59. Williams, P., M. Whitfield, J. Biggs, S. Bray, G. Fox, P. Nicolet, and D. Sear. 2004. Comparative biodiversity of rivers, streams, ditches and ponds in an agricultural landscape in Southern England. Biol. Conserv. 115(2): 329-341, doi: 10.1016/S0006-3207(03)00153-8

60. Wernberg, T., and others. 2016. Climate-driven regime shift of a temperate marine ecosystem. Science. 353(6295): 169-172, doi: 10.1126/science.aad8745

61. Woolway, R. I., E. Jennings, T. Shatwell, M. Golub, D.C. Pierson, and S.C. Maberly. 2021a. Lake heatwaves under climate change. Nature. 589: 402-407, doi: 10.1038/s41586-020-03119-1

62. Woolway, R.I., B.M. Kraemer, J. Zscheischler, and C. Albergel. 2021b. Compound hot temperature and high chlorophyll extreme events in global lakes. Environ. Res. Lett. 16(12): 124066, doi: 10.1088/1748-9326/ac3d5a

63. Woolway, R.I., C. Albergel, T.L. Frölicher, and M. Perroud. 2022. Severe Lake Heatwaves Attributable to Human-Induced Global Warming. Geophys. Res. Lett. 49(4): e2021GL097031, doi: 10.1029/2021GL097031

64. Wu, H., B. Hao, H. Jo, Y. Cai. 2021. Seasonality and species specificity of submerged macrophyte biomass in shallow lakes under the influence of climate warming and eutrophication. Front. Plant Sci. 12: 678259, doi: 10.3389/fpls.2021.678259

825 **TABLES**

826 **Table 1.** *Temporal versus spatial variation in DO Saturation*

		Temporal Variation in DO Saturation		***Spatial Variation in DO Saturation***	
Layer	*Pond*	*CV (%)* Mean	*CV (%)* Range	*CV (%)* Mean	*CV (%)* Range
Surface	Reference	28.9	20.2 – 34.4	5.9	1.8 – 11.3
	Nutrient Addition	22.8	20.6 – 28.8	4.4	2.1 – 9.5
Bottom	Reference	34.4	24.1 – 45.6	7.5	2.0 – 16.3
	Nutrient Addition	26.8	22.1 – 40.3	7.5	2.0 – 16.9

827

828

829

830 **FIGURES**

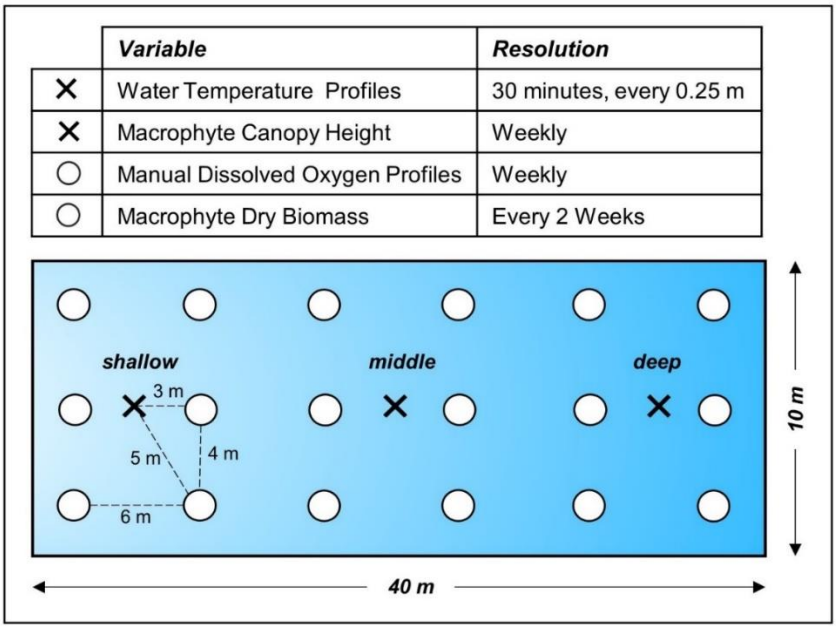

831

832 **Figure 1.** Spatial and temporal resolution of measured variables and sample site locations.

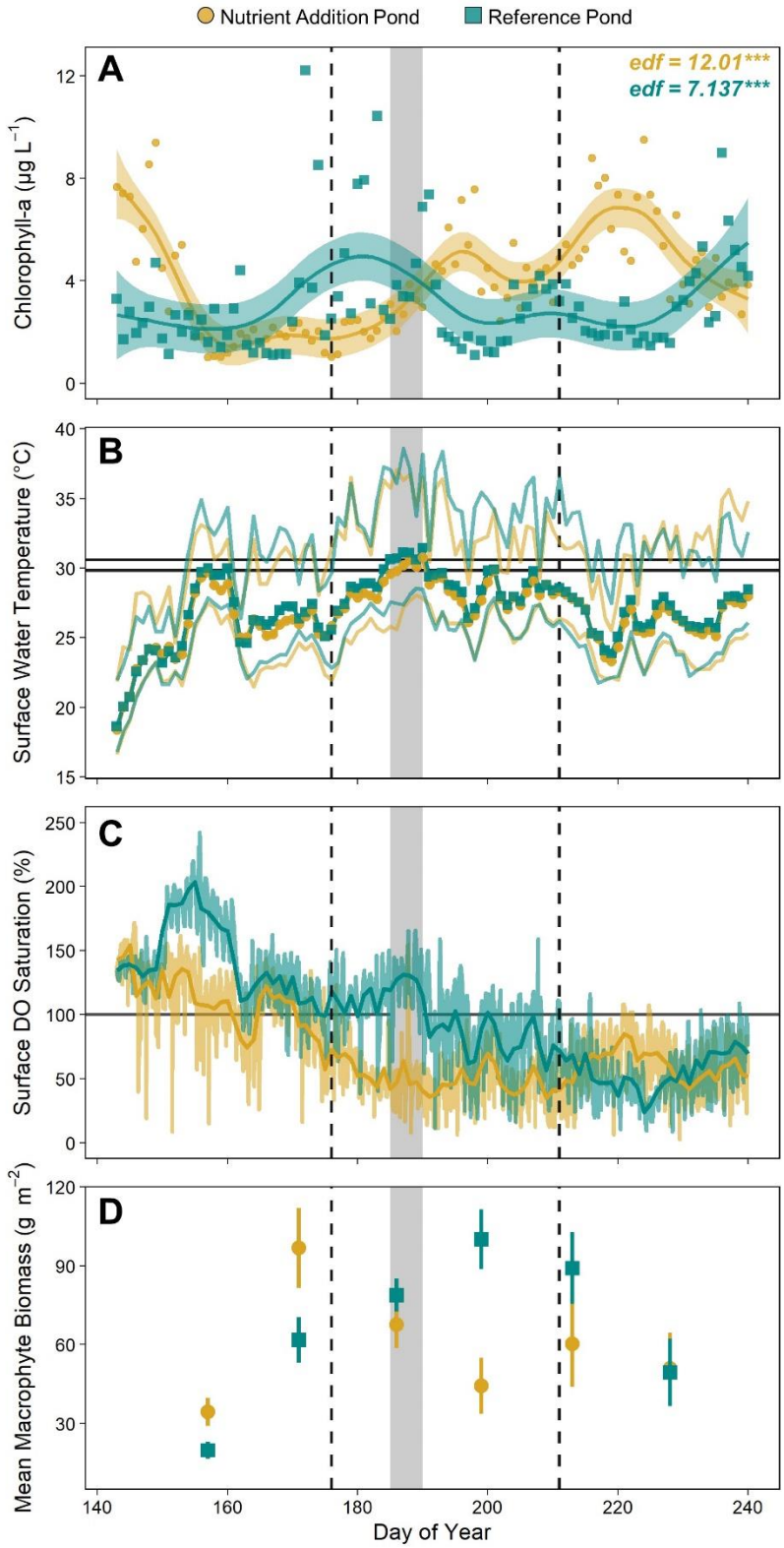

833

834 **Figure 2.** (A) Timeseries of surface chlorophyll-*a* concentrations. Values from each pond were
835 GAM-fit to highlight temporal trends. The asterisks next to the effective degrees of freedom

(edf) correspond to the estimated p-value, with *** denoting $p < 0.001$. (B) Timeseries of mean daily surface (0-0.25 m) water temperature. Surface sensors at the deep and middle sites were used for these pond averages. The 95th percentile surface water temperature thresholds are noted in horizontal lines for the nutrient addition (29.8°C) and reference (30.6°C) ponds. (C) High frequency surface dissolved oxygen (DO) saturation at the deep site of each pond over the study period. The daily mean is plotted in a darker line. The horizontal grey line marks 100 percent saturation. (D) Time series of mean macrophyte biomass in each pond. Error bars mark the standard error of the mean. Across all panels, dashed lines mark the timing of nutrient additions (DOY 176, 211) and the grey box highlights the aquatic heat event (DOY 185-190).

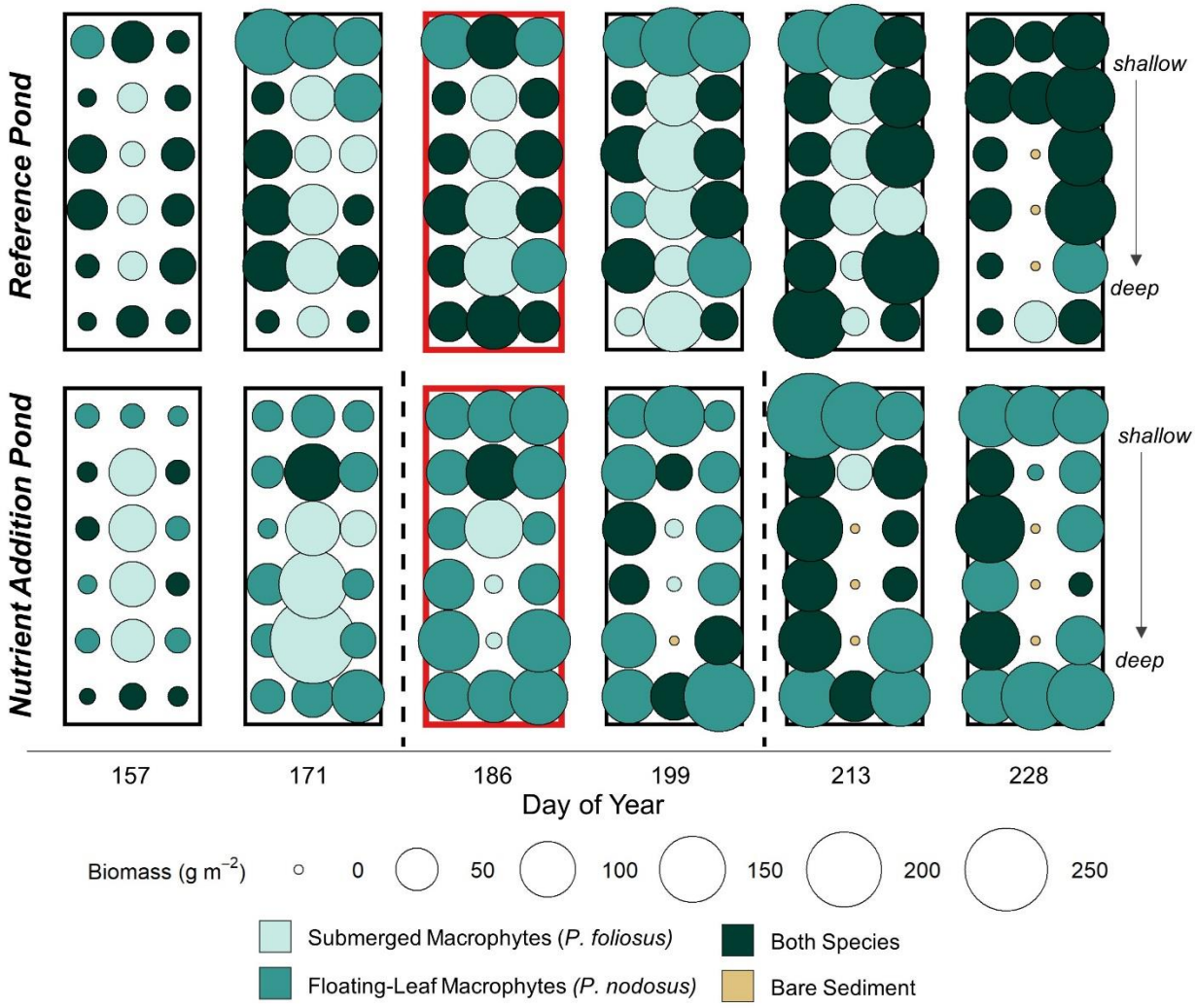

Figure 3. Spatial and temporal variation in macrophyte dry biomass and community composition. Biomass was sampled during the aquatic heat event (DOY 185-190), as noted by the thicker, red pond outline on DOY 186. Dashed lines mark nutrient additions on DOY 176 and 211.

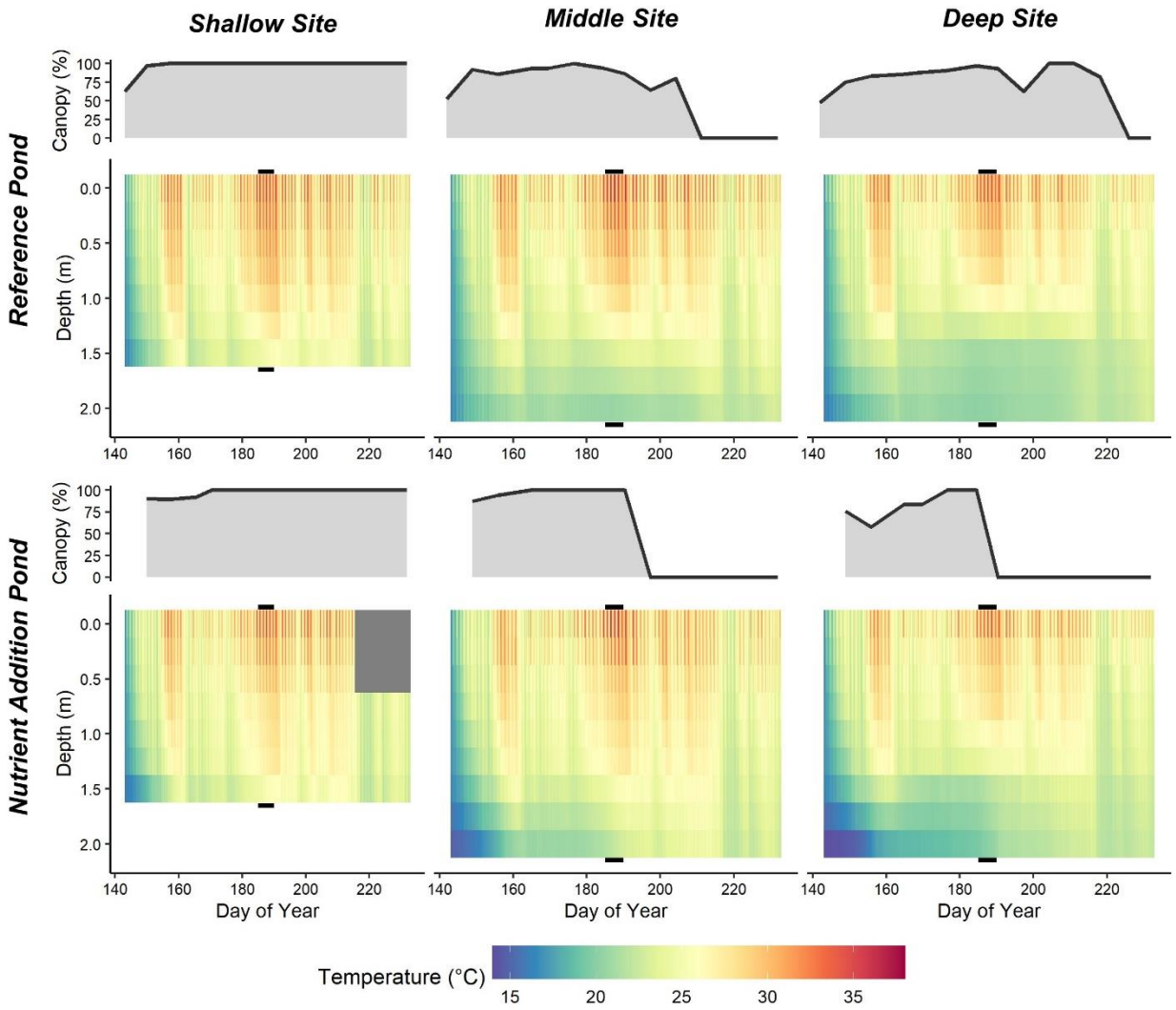

Figure 4. Spatial and temporal variation in macrophyte canopy height and temperature profiles. Canopy height is plotted as a percent of the water column height. Black, horizontal lines mark an aquatic heat event from DOY 185-190. High frequency water temperature loggers were placed every 0.25 m of the water column up to 1.5 m and then every 0.5 m to the bottom. Temperature values at 1.75 m were interpolated for the sake of visualization. Several surface sensors (0-0.5 m) from the shallow site of the nutrient addition pond lost power following DOY 215 (grey box). An initial canopy height measurement is missing from the nutrient addition pond because the water was not sufficiently clear to see and measure the top of the canopy. The canopy height was less than 1 m or 50-75% of the water column at this time.

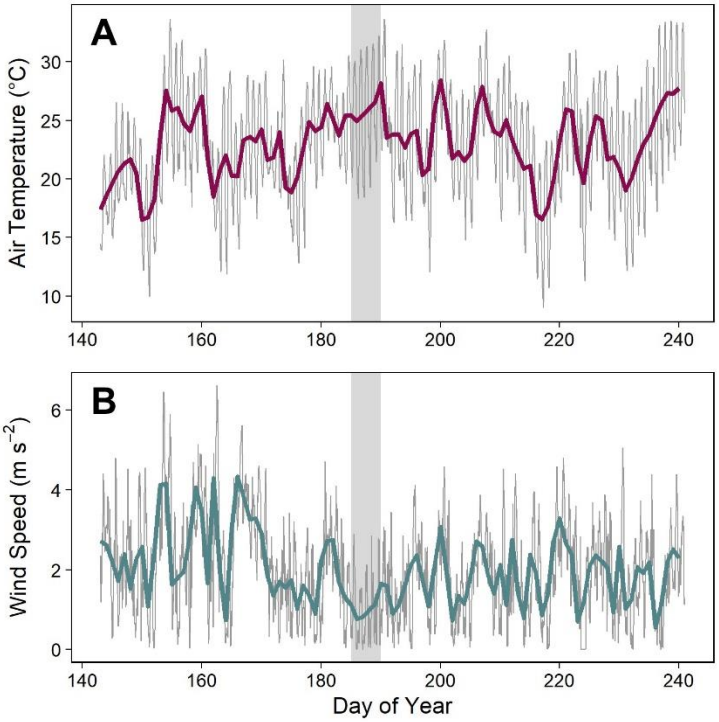

Figure 5. Air temperature (A) and windspeed (B) over the study period. Daily mean values are plotted in thicker lines over the hourly time series.

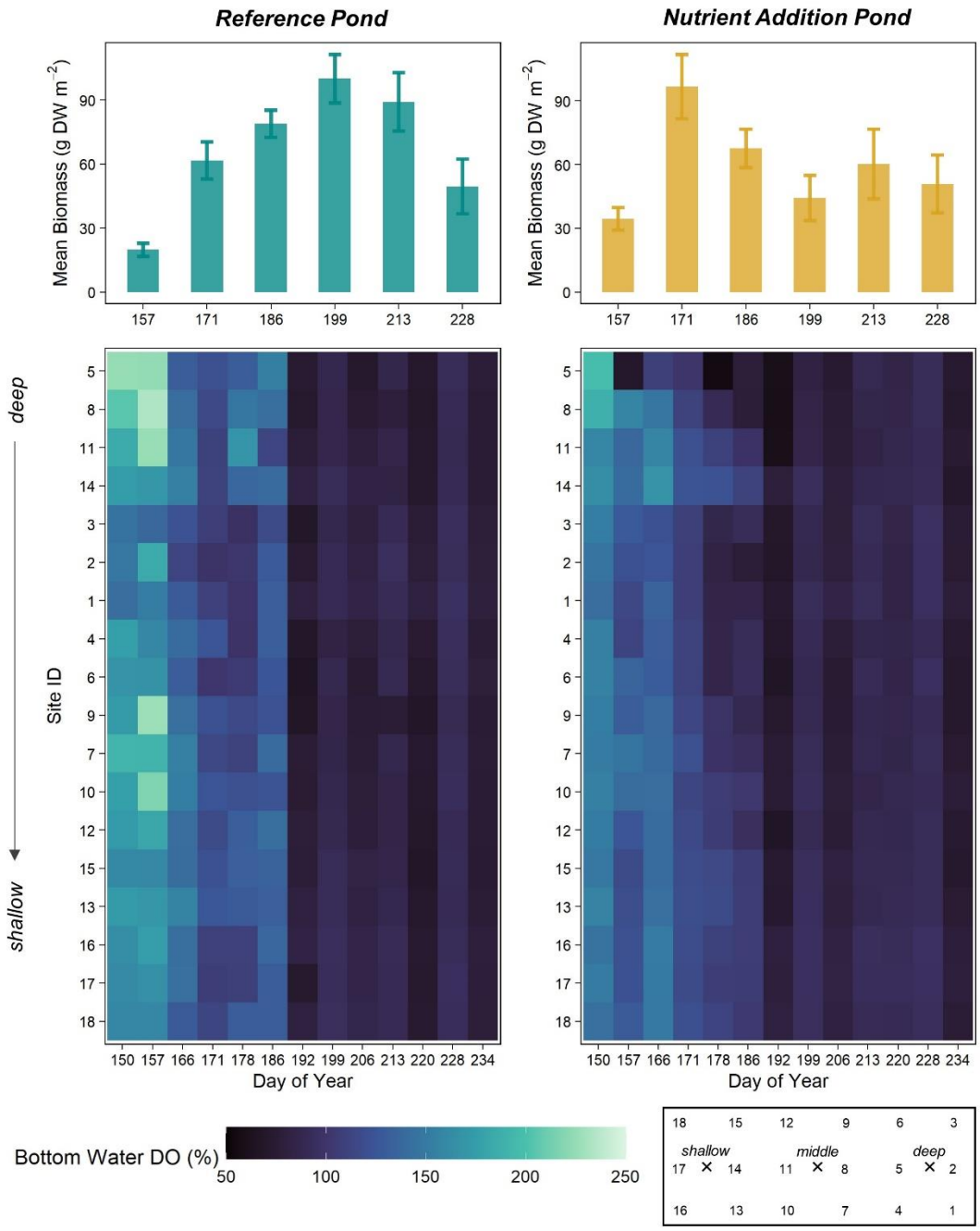

Figure 6. Spatiotemporal variation in bottom water dissolved oxygen (DO) saturation. Sampling sites are ordered approximately from the deepest to most shallow locations. The pond-averaged biomass values are plotted above. Error bars represent the standard error of the mean.

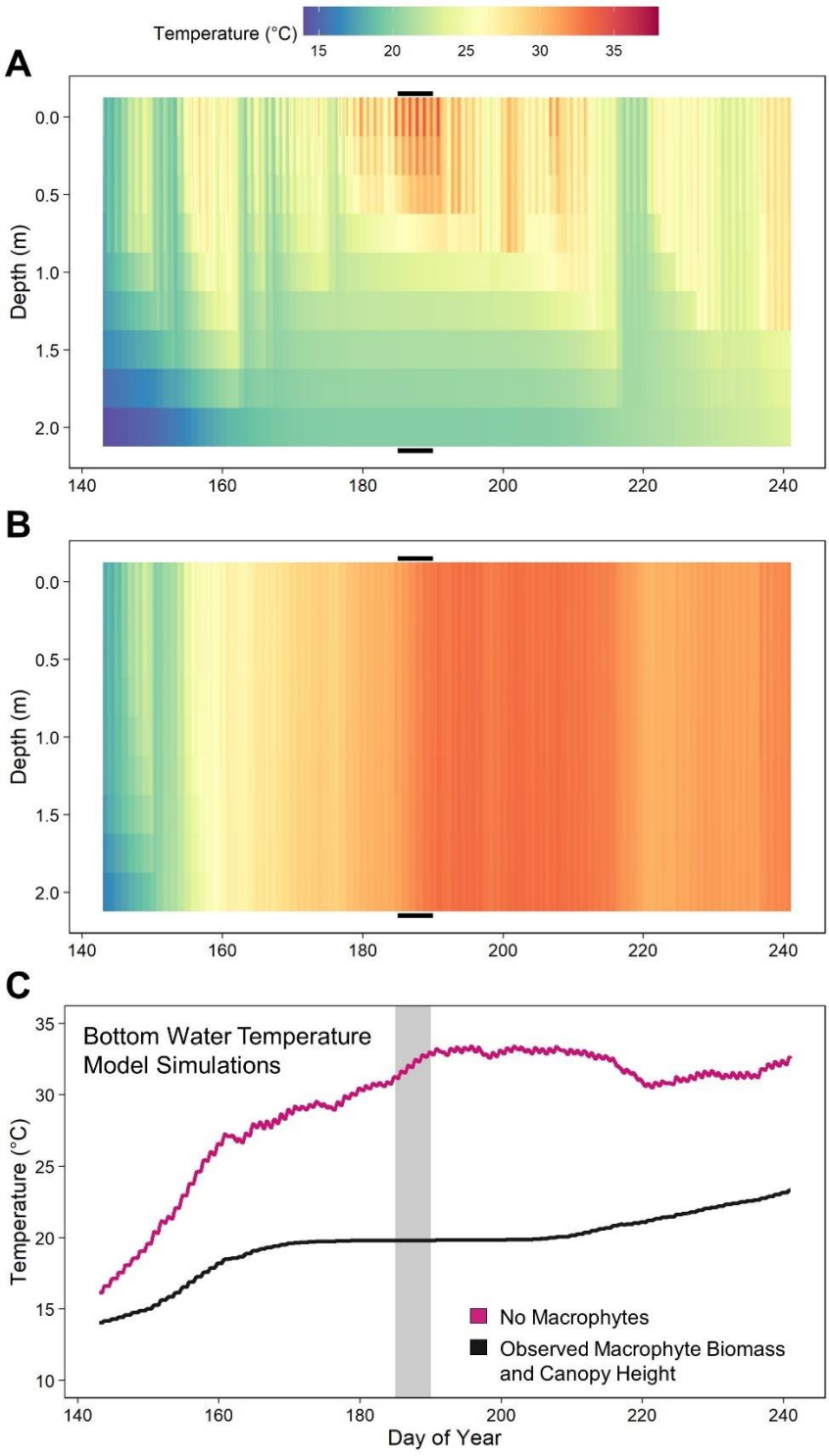

Figure 7. Model simulation results contrasting a no macrophyte scenario with the observed macrophyte coverage from the reference pond. Predicted temperature profiles with (A) observed macrophyte biomass and canopy height versus (B) no macrophytes present in the reference pond. Black, horizontal lines mark an aquatic heat event (DOY 185-190). (C) Timeseries of predicted daily mean bottom water (2m) temperatures with no macrophytes versus observed macrophyte biomass and canopy height.

Appendix S1

Macrophyte-hydrodynamic interactions mediate stratification and dissolved oxygen dynamics in ponds

Ellen A. Albright[1,2], Robert Ladwig[2], and Grace M. Wilkinson[1,2]

[1] Iowa State University, Ames, Iowa, USA

[2] Center for Limnology, University of Wisconsin-Madison, Madison, Wisconsin, USA

Corresponding author: Ellen A. Albright (ealbright2@wisc.edu)

Introduction

The appendix contains additional methods text detailing the algorithms and approach for the hydrodynamic model as well as an overview of calibrated model parameters (Table S1) and simulation input data for testing heat event response under variable macrophyte scenarios (Table S2). Model fit is illustrated in Figure S6.

Figure S1 provides an example of individual dissolved oxygen (DO) saturation profiles to illustrate there was no evidence of mid-depth DO maxima. We provide time series of estimated thermocline depth (Figure S2) and Lake Number (Figure S3) for each pond as well as time series of bottom water temperatures at each sampling site on each pond (Figure S4). We further provide supplementary visualizations for our DO data, specifically time series of surface and bottom water DO saturation and the difference between surface and bottom water DO (Figure S5).

Model Equations and Approach

Model description

A one-dimensional, integral energy model was developed to simulate the temperature, heat flux and stratification dynamics in small, vegetated ponds. Model algorithms are based on the MINLAKE model (Ford and Stefan 1980; Riley and Stefan 1988; Herb and Stefan 2004).

Heat transport is implemented through the one-dimensional temperature diffusion equation:

(Eq. 1) $$\frac{\partial T}{\partial t} = \frac{\partial}{\partial z}\left(K_z \frac{\partial T}{\partial t}\right) + \frac{H(z)}{\rho_w c_p} + \frac{H_{geo}(z)}{\rho_w c_p}$$

where K_z is the vertical turbulent diffusion coefficient, H is internal heat generation due to incoming solar radiation, ρ_w is water density, c_p is specific heat content of water, and H_{geo} is internal geothermal heat generation.

Internal heat generation is implemented as:

(Eq. 2) $$H(z) = (1-\alpha) I_s^{-((k_d + k_m)z)}$$

where α is the water albedo, I_s is total incident short-wave radiation, and k_d is a light attenuation coefficient and k_m is the light attenuation coefficient due to macrophyte biomass.

For the upper, surface boundary condition we assume a Neumann type for the temperature diffusion equation:

(Eq. 3) $$H_{net} = \rho_w c_p \left(K_z \frac{\partial T}{\partial t}\right)$$

where H_{net} is the net heat flux exchange between atmosphere and water column:

(Eq. 4) $$H_{net} = H_{lw} + H_{lwr} + H_v + H_c$$

where H_{lw} is the incoming long-wave radiation, H_{lwr} is emitted radiation from the water column, H_v is the latent heat flux, and H_c is the sensible heat flux. Implementations to estimate the respective heat fluxes were taken from Livingstone and Imboden (1989) and Goudsmit et al.

(2002). Latent and sensible heat fluxes were calculated using the atmospheric stability algorithms from Verburg and Antenucci (2010).

The lower, sediment boundary condition was prescribed as:

(Eq. 5) $$\left(K_z \frac{\partial T}{\partial t}\right) = 0$$

The model algorithm is modularized into three components: (a) heat generation from boundary conditions and vertical diffusion, (b) turbulent mixing up to the mixed layer depth, and (c) convective overturn to account for density instabilities.

(a) Heat generation from boundary conditions and vertical diffusion

In the first step the heat fluxes H and H_{geo} are applied over the vertical water column. The atmospheric heat flux, H_{net}, is applied to the surface layer.

Simultaneously, vertical turbulent diffusion between adjacent grid cells is calculated. Here, we applied the implicit Crank-Nicholson scheme. The vertical turbulent diffusion coefficient K_z is calculated based on the empirical equations by Hondzo and Stefan (1993) for lakes in Minnesota as a function of the buoyancy frequency:

(Eq. 6) $$K_z = a_k (N^2)^{-0.43}$$

where a_k is an empirical factor accounting for the surface area of the lake A_s:

(Eq. 7) $$a_k = 0.00706 (A_s)^{0.56}$$

and N^2 is the squared buoyancy frequency:

(Eq. 8) $$N^2 = \frac{g}{\rho_w} \frac{\partial \rho_w}{\partial z}$$

Values of N^2 less than 7.0 10^{-5} s^{-2} were set to 7.0 10^{-5} s^{-2}.

(b) Mixed layer depth

In the third step, we quantified the depth where the amount of external kinetic energy by wind shear stress equals the internal potential energy of the water column. Up to this mixed layer

depth, z_{ml}, adjacent layers are subsequently mixed to account for a wind shear stress acting over the vertical water column. Here, the kinetic energy *KE* is described as:

(Eq. 9) $$KE = \tau u^* \Delta t$$

where τ is the surface turbulent shear stress, and u^* is the surface shear velocity, which was calculated from wind velocity as:

(Eq. 10) $$u^* = \sqrt{\frac{C_{10}\rho_a}{\rho_w}} U_2$$

where C_{10} is the wind stress coefficient dependent on the measured wind speed U_2 at 2 m height above the water surface, and ρ_a is the density of air, respectively (Herb and Stefan, 2005).

The dissipation of turbulent kinetic energy (DKE) by macrophytes is incorporated as:

(Eq. 11) $$DKE_z = (\rho_w \hat{a} C_d)(u^*)^3 \Delta z \Delta t$$

where $\hat{a}$ is the ratio of plant surface area per unit volume water and C_d is the plant form drag coefficient.

The potential energy of the water column for each layer over the depth is calculated as:

(Eq. 12) $$PE_z = g Z_z (Z_{z+1} - Z_{cv}) \Delta \rho$$

where g is gravitational acceleration, z_{cv} is the center of volume depth, and $\Delta\rho$ is a density change from the current layer to the next layer below.

The mixed layer depth z_{ml} is calculated by incrementally increasing the comparison between the difference of total kinetic energy *KE* to the dissipation of KE by macrophytes, and the internal potential energy *PE* as:

(Eq. 14) $$z_{ml} \rightarrow PE_{z+1} > (KE - DKE_z)$$

(c) Convective overturn

In the fourth step, any density instabilities over the vertical water column are mixed with a first stable layer below an unstable layer. Here, we applied an area weighed mean of temperature between adjacent layers to calculate the temperature of the mixed layer.

Appendix References

1. Ford, D.E., and H.G. Stefan. 1980. Thermal predictions using an integral energy model. J. Hydraul. Div. ASCE 106(1). 39-55, doi: 10.1061/JYCEAJ.0005358

2. Goudsmit, G.H., H. Burchard, F. Peeters, and A. Wüst. 2002. Application of k-e turbulence models to enclosed basins: The role of internal seiches. J. Geophys. Res. 107. C12. 3230, doi:10.1029/2001JC000954

3. Herb, W.R., and H.G. Stefan. 2004. Temperature stratification and mixing dynamics in a shallow lake with submersed macrophytes. Lake Reserv. Manag. 20(4): 296-308, doi: 10.1080/07438140409354159

4. Herb, W.R., and H.G. Stefan, 2005. Dynamics of vertical mixing in a shallow lake with submersed macrophytes. Water Resour. Res. 41. W02023, doi:10.1029/2003WR002613

5. Hondzo, M., and H.G. Stefan. 1993. Lake water temperature simulation model. J. Hydraul. Eng. 119(11). 1251-1273, doi: 10.1061/(ASCE)0733-9429(1993)119:11(1251)

6. Livingstone, D., and D. Imboden. 1989. Annual heat balance and equilibrium temperature of Lake Aegeri, Switzerland. Aquat. Sci. 51(4): 351-369, doi: 10.1007/BF00877177

7. Riley, M., and H.G. Stefan. 1988. MINLAKE: A dynamic lake water quality simulation model. Ecol. Model. 43. 155-182, doi: 10.1016/0304-3800(88)90002-6

8. Verburg, P., and J.P. Antenucci. 2010. Persistent unstable atmospheric boundary layer enhances sensible and latent heat loss in a tropical great lake: Lake Tanganyika. Journal of Geophysical Research 115. 1-13. doi: 10.1029/2009JD012839

Table S1. *Calibrated model parameter values*

Variable	Description	Value	Parameterization
C_d	Wind momentum drag	0.0013	Calibration to field data
K_m	Macrophyte light extinction coefficient	0.04	Calibration to field data
$C_{d\ plant}$	Macrophyte momentum drag coefficient	1	Herb and Stefan (2004)
$\hat{a}$	Macrophyte area to volume	0.5	Calibration to field data
Wind factor	Wind speed multiplier	1	Best field calibration did not use wind speed or diffusion rate multipliers (so factors equal to 1)
Diffusion factor	Diffusion rate multiplier	1	
Short wave factor	Shortwave radiation multiplier	0.9	Calibration to field data
H_{geo}	Sediment heating coefficient	0	Calibration to field data
ρ_m	Macrophyte density	30	Calibration to field data

Table S2. *Input macrophyte data for model simulations*

Field Data – Reference Pond															
DOY	129	143	150	157	166	171	178	186	192	199	206	213	220	228	234
Canopy (m)	0.5	1	1.5	1.6	1.6	1.6	1.6	1.6	1.45	1	1.6	1.8	1/4	0.5	0.5
Biomass (g m^2)	NA	NA	NA	14.5	NA	48.4	NA	101.4	NA	73.6	NA	15.4	NA	22.4	NA
Simulation – No Macrophytes in Reference Pond															
DOY	129	143	150	157	166	171	178	186	192	199	206	213	220	228	234
Canopy (m)	0	0	0	0	0	0	0	0	0	0	0	0	0	0	0
Biomass (g m^2)	0	0	0	0	0	0	0	0	0	0	0	0	0	0	0

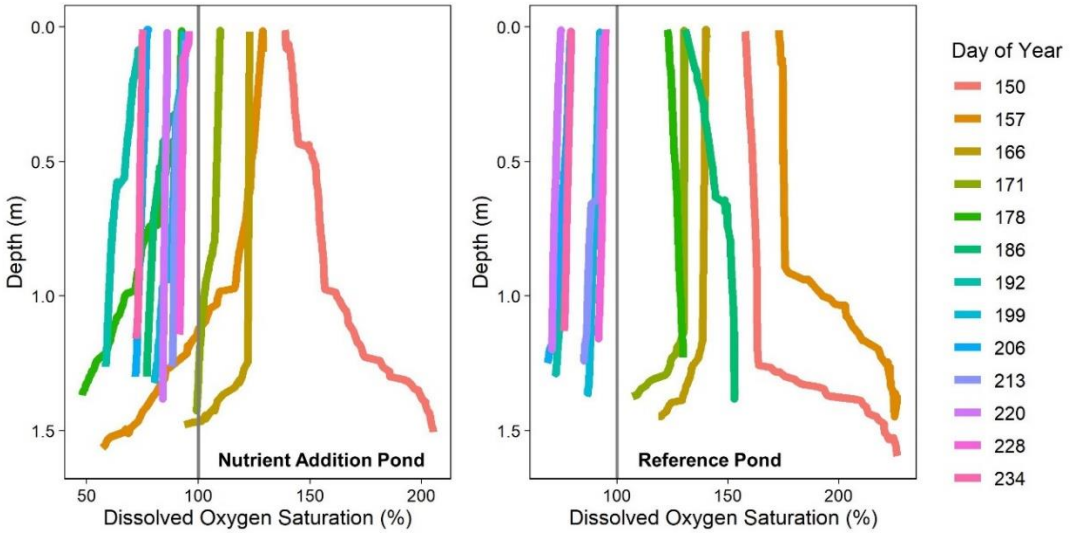

Figure S1. Examples of individual dissolved oxygen (DO) saturation profiles near deep sites. Profiles are color-coded by the DOY of the sampling event. These profiles were taken in the deeper, central region of the ponds. The vertical grey line highlights 100 percent saturation.

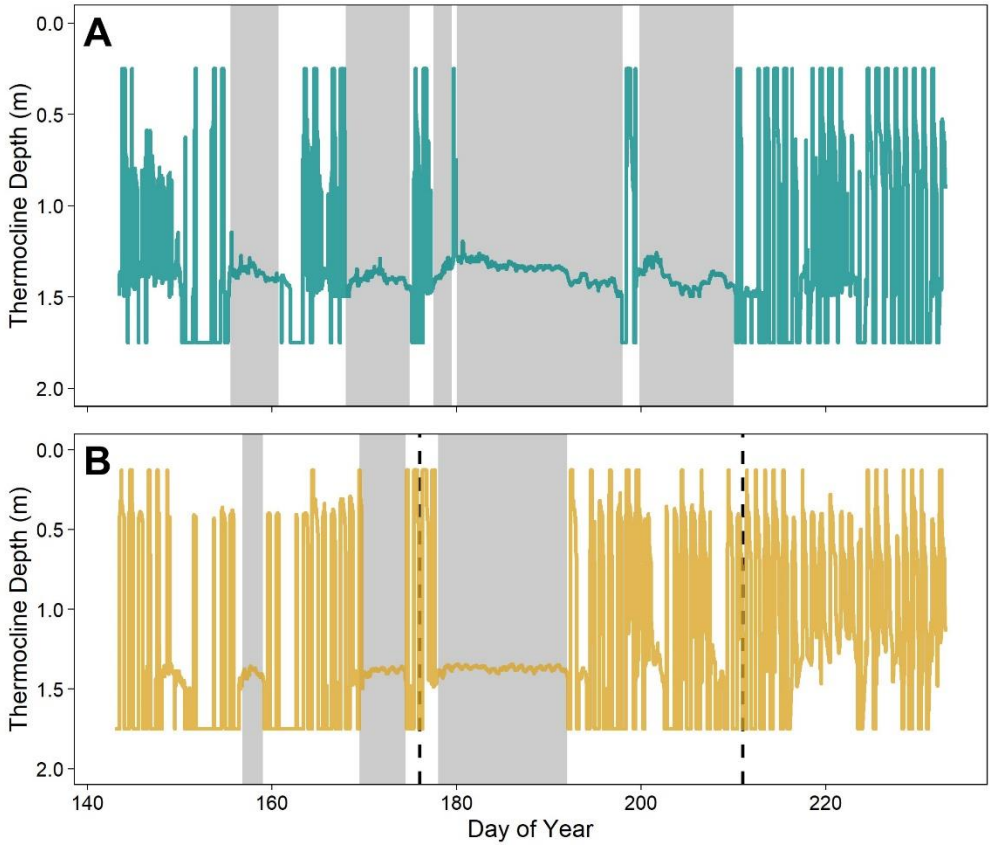

Figure S2. Estimated thermocline depth by pond. Periods of a stable thermocline for the reference (A) and nutrient addition (B) ponds are noted in the grey shaded boxes. Nutrient additions are noted with dashed black lines. Estimated thermocline values oscillating rapidly between the near surface and bottom waters were not considered time of stable stratification.

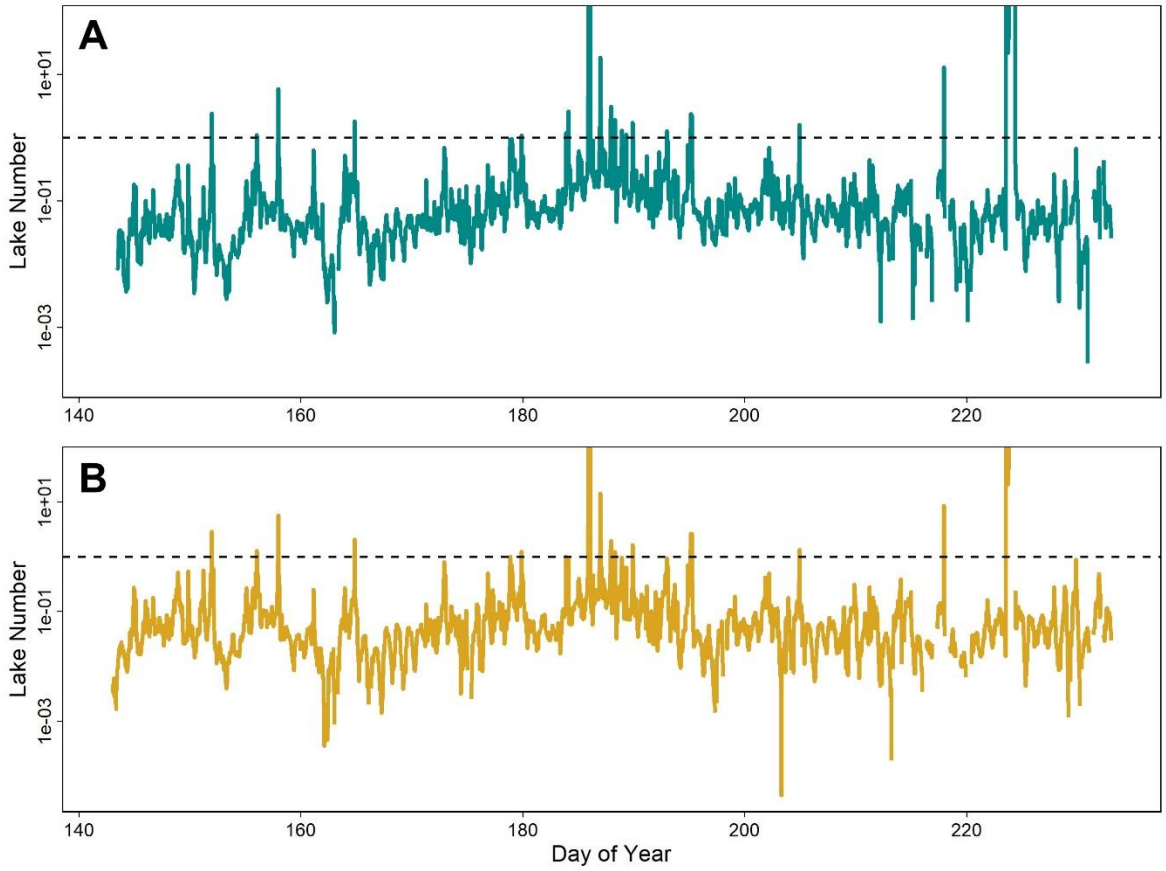

Figure S3. Time series of Lake Number for the reference (A) and nutrient addition (B) ponds. A value of one (horizontal dashed line) indicates that the internal stability of the water column is balanced with wind stress. Values greater than one indicate that the water column is strongly stratified while values less than one mean that stratification is weak compared to wind shear stress.

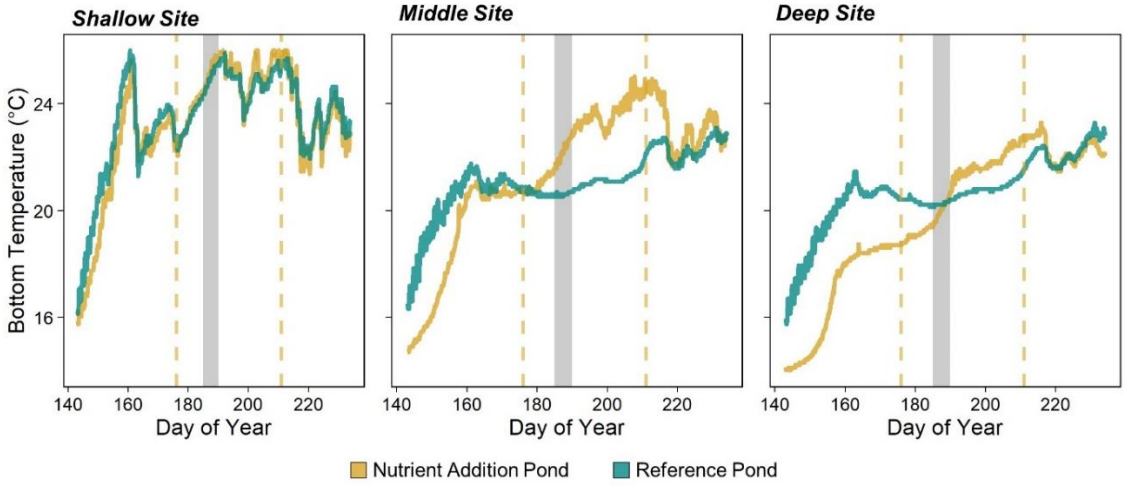

Figure S4. Bottom water temperature time series across sampling sites. The grey box marks an aquatic heat event from DOY 185-190. Yellow dashed lines indicate the nutrient additions on DOY 176 and 211.

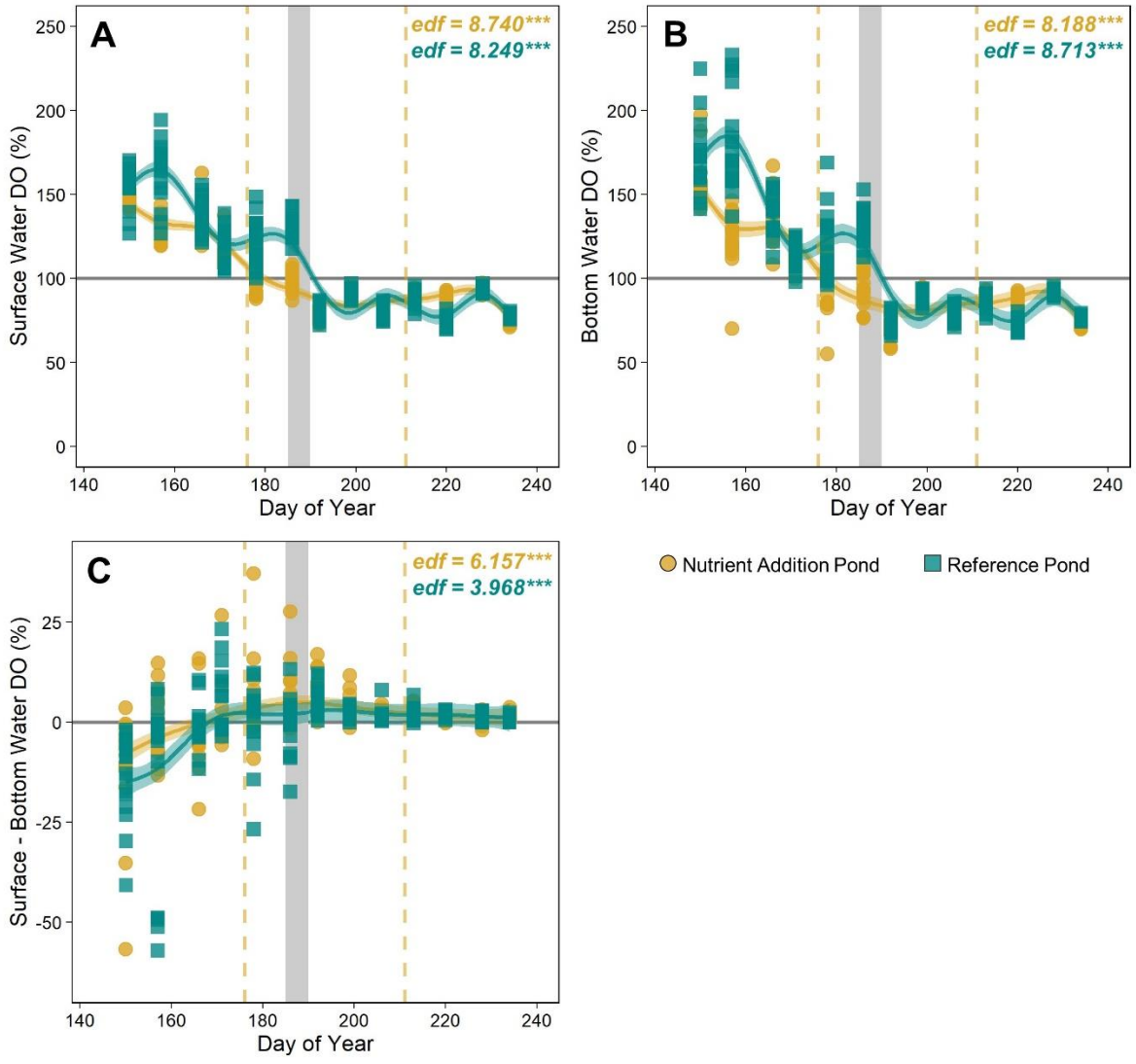

Figure S5. Time series of surface and bottom water dissolved oxygen (DO) saturation and the difference between the two. (A) Surface water DO saturation, (B) bottom water DO saturation, and (B) the difference between surface and bottom water DO saturation is based on weekly profiles at 18 sites across each pond. Negative values of delta-DO indicate greater DO saturation in the bottom waters while positive values mean DO is higher in the surface layer. Values from each pond were GAM-fit to highlight temporal trends. The asterisks next to the effective degrees of freedom (edf) correspond to the estimated p-value, with *** denoting $p < 0.001$. Across both panels, dashed yellow lines mark the timing of nutrient additions and the grey box highlights the aquatic heat event.

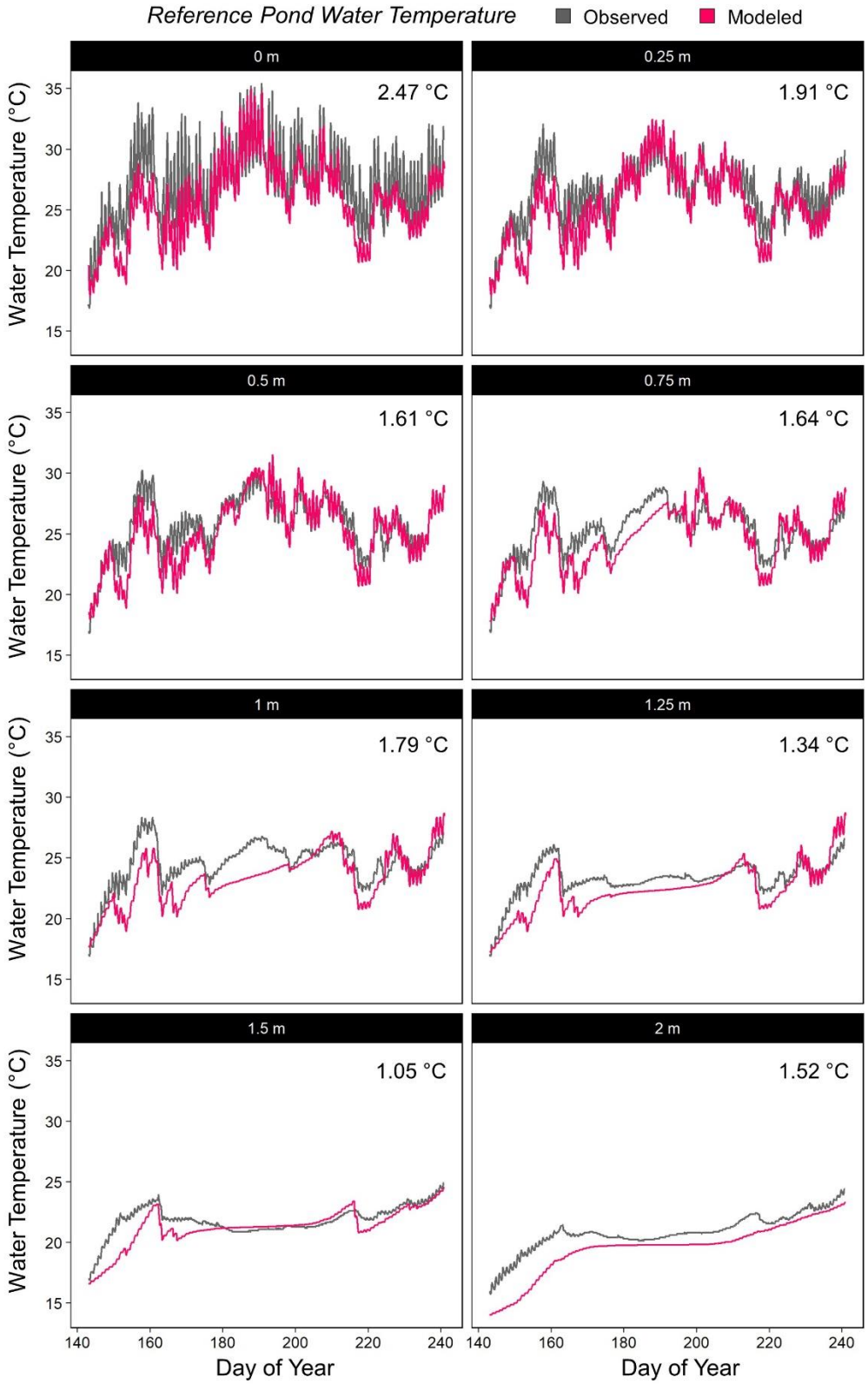

Figure S6. Model fit at discrete depths in the reference pond. Predicted water temperatures from the hydrodynamic model are plotted against the observed temperatures at the same depths. The root mean square error (RMSE, °C) are noted in the top right corner of each panel